

# Accretion Geometry of Black Hole X-ray Binaries: Insights from X-ray Observations

Honghui Liu<sup>1\*</sup>

<sup>1\*</sup>Institut für Astronomie und Astrophysik, Eberhard-Karls Universität  
Tübingen, Tübingen, D-72076, Germany.

Corresponding author(s). E-mail(s): [honghui.liu@uni-tuebingen.de](mailto:honghui.liu@uni-tuebingen.de);

## Abstract

The accretion-ejection activities of black holes play a vital role in shaping the Universe. Bright and recurrent black hole X-ray binaries are ideal objects for studying accretion physics across a wide range of accretion rates, providing insights into the understanding of their supermassive counterparts. This short review summarizes X-ray techniques capable of measuring accretion geometry, our current understanding, and open questions. In particular, X-ray spectroscopic studies indicate that the accretion disk can extend close to the innermost stable circular orbit in the bright hard state. Some hints of disk-corona-jet connections are also discussed.

**Keywords:** X-ray binaries, Black holes, accretion

## 1 Introduction

Black hole (BH) X-ray binaries (XRBs) are systems in which a stellar-mass black hole, with typical masses ranging from several to tens of solar masses ( $M_{\odot}$ ), is accreting matter from its companion star (see Figure 1). The accreted matter forms a disk-like accretion flow around the central BH. This process is highly efficient at converting gravitational energy into radiation, producing strong electromagnetic emission. In the case of accretion onto stellar-mass BHs, the emission is predominantly in the X-ray band. These X-ray photons are particularly valuable, as they originate from the innermost regions of the accretion flow near the BH. As a result, the X-ray signal serves as a powerful tool for studying BHs and the nearby strong gravity region (De Rosa et al., 2019; Reynolds, 2021; Bambi et al., 2021).

The first confirmed BH XRB, Cygnus X-1 (Murdin and Webster, 1971), was discovered during the early years of X-ray astronomy by instruments onboard sounding rockets (Bowyer et al., 1965; Bolton, 1972). Since then, space-based X-ray all-sky monitors (e.g., RXTE, MAXI) have continued to discover new BH XRB candidates. As of today, around 80–100 candidates have been identified in the Galaxy, of which approximately 20 have been dynamically confirmed to host stellar-mass black holes.<sup>1</sup> (Tetarenko et al., 2016; Corral-Santana et al., 2016; Neumann et al., 2023; Avakyan et al., 2023).

Early X-ray satellites revealed complex spectral and timing behaviors, which led to the initial definition of spectral states in BH XRBs (Tanaka and Lewin, 1995). Later missions with high energy and timing resolution, such as *RXTE* (2–60 keV), *XMM-Newton* (0.15–12 keV), *Chandra* (0.1–10 keV), *INTEGRAL* (3 keV – 10 MeV), *Swift* (0.2–10 keV for XRT and 15–150 keV for BAT), *Suzaku* (0.2–12 keV for XIS and 10–600 keV for HXD), *NuSTAR* (3–79 keV), *NICER* (0.2–12 keV), *Insight-HXMT* (1–250 keV), and *AstroSat* (0.3–100 keV), have provided a more comprehensive and unified understanding of these states, based on their combined spectral and timing properties (see Remillard and McClintock, 2006; McClintock and Remillard, 2006; Done et al., 2007; Belloni, 2010; Belloni and Motta, 2016, for detailed reviews).

In addition to the high-quality data provided by these missions, there has been significant progress over the past 15 years in modeling the X-ray signals from BH XRBs, particularly regarding the spectral and timing signatures of the relativistic reflection component (e.g., García and Kallman, 2010; Ingram et al., 2019; Bambi et al., 2021, and see Sec. 3.1) and the interpretation of quasi-periodic oscillations (e.g., Ingram and Motta, 2019, and see Sec. 3.2). These improvements collectively contribute to a better understanding of the accretion flow geometry, which is essential for addressing more fundamental questions such as measuring black hole spins (e.g., Reynolds, 2021; Liu et al., 2023a; Draghis et al., 2024) and potentially even testing general relativity (e.g., Bambi, 2017; Liu et al., 2018, 2019; Bambi, 2024b).

More recently, the launch of the Imaging X-ray Polarimetry Explorer (IXPE) in 2021 opened a new observational window via X-ray polarimetry. Its findings are already challenging our pre-polarimetry understanding of accretion geometry and dynamics (see Section 4). Gravitational wave (GW) detections by LIGO, Virgo, and KAGRA have also provided insights into populations of black holes found in BH-BH/BH-NS binaries, some of which may also be stellar-remnant black holes (Abbott et al., 2021a,b, 2023). Interestingly, the black holes detected through GWs appear to be more massive (e.g., Abbott et al., 2023; Liotine et al., 2023) and to spin more slowly (e.g., Fishbach and Kalogera, 2022; Connors et al., 2024) than those found in XRB systems, indicating different BH populations or evolutionary pathways.

In this review, we summarize our current understanding of the accretion geometry in BH XRBs and highlight open questions that remain to be addressed. In Section 2, we describe the main spectral components and states of BH XRBs. Section 3 outlines the X-ray techniques used to study accretion geometries. In Section 4, we summarize the inferred accretion geometry based on current X-ray observations.

---

<sup>1</sup>Two useful catalogs include: (1) XRBcat: <http://astro.uni-tuebingen.de/~xrbcat/index.html>; (2) BlackCAT: <https://www.astro.puc.cl/BlackCAT/index.php>.

## 2 X-ray emission and spectral states

The X-ray spectrum of BH XRBs typically consists of several components, as illustrated in Figure 1 in the framework of the disk-corona model. The central BH is surrounded by an optically thick, geometrically thin accretion disk (Shakura and Sunyaev, 1973; Novikov and Thorne, 1973). The accretion disk emits blackbody emission locally, and the spectrum of the whole disk is a multi-temperature blackbody (e.g., disk thermal emission, Mitsuda et al., 1984). The blackbody temperature generally increases for radii closer to the black hole, and can reach 1–2 keV at the innermost stable circular orbit (ISCO) radius for BH XRBs when they are accreting at appreciable fractions of their Eddington limits. The disk blackbody component typically peaks in soft X-ray band (e.g., at few keV or less, Fig. 1). Near the BH, there exists a cloud of hot plasma (with a temperature of  $\sim 100$  keV), commonly referred to as the corona (Thorne and Price, 1975; Shapiro et al., 1976). The corona can Compton up-scatter seed photons from the disk, or from internal processes within the corona itself (Malzac and Belmont, 2009; Poutanen and Vurm, 2009), producing a non-thermal power-law-like emission that extends into the hard X-ray band. While the basic structure of the accretion disk is relatively well understood, the geometry and formation mechanism of the corona remain less certain (see Liu and Qiao, 2022; Bu and Zhang, 2023, for recent reviews).

The coronal emission can illuminate the optically-thick accretion disk and be reprocessed to produce the *reflection* component (George and Fabian, 1991; García and Kallman, 2010). In the rest-frame of the accretion disk, the reflection spectrum is characterized by narrow fluorescent emission lines (the strongest one is typically the iron  $K\alpha$  line at 6.4–7 keV) and a Compton reflection hump that peaks around 20–30 keV. The observed reflection spectrum is broadened by relativistic effects (e.g., Doppler shifts and gravitational redshift, Fabian et al. 1989) and carries valuable information about the accretion system (see details in Sec. 3.1).

BH XRBs can generally be divided into persistent and transient sources, with the latter comprising the majority (Corral-Santana et al., 2016). Transient BH XRBs spend most of their time in the *quiescent* state, characterized by low X-ray luminosity (e.g.,  $L_X < 10^{33}$  erg s $^{-1}$ ) and a hard, non-thermal X-ray spectrum (Kong et al., 2002; Corbel et al., 2006; McClintock and Remillard, 2006; Reynolds et al., 2014). Figure 2 shows typical lightcurves of a transient BH XRB (GX 339-4) and a persistent source (Cygnus X-1). Transient sources can undergo outbursts triggered by instabilities in the outer disk (Lasota, 2001; Coriat et al., 2012) during which their X-ray luminosity can increase by several orders of magnitude (reaching  $L_X = 10^{37} - 10^{39}$  erg s $^{-1}$ ). Persistent sources remain continuously bright and never enter quiescence.

The outburst can also be traced using the hardness-intensity diagram (HID, Belloni et al. 2005; Belloni 2010). In this diagram, the hardness can be simply defined as the ratio of count rates in a hard X-ray band to those in a soft X-ray band. It broadly indicates the spectral shape of the source. The intensity can be the total count rate of the detector, which is related to the source luminosity or mass accretion rate. There is no strict definition of the hard/soft X-ray bands or the intensity. Alternative diagrams, such as the rms-intensity diagram (Muñoz-Darias et al., 2011), can also be used to track the outburst using information from both the source luminosity and

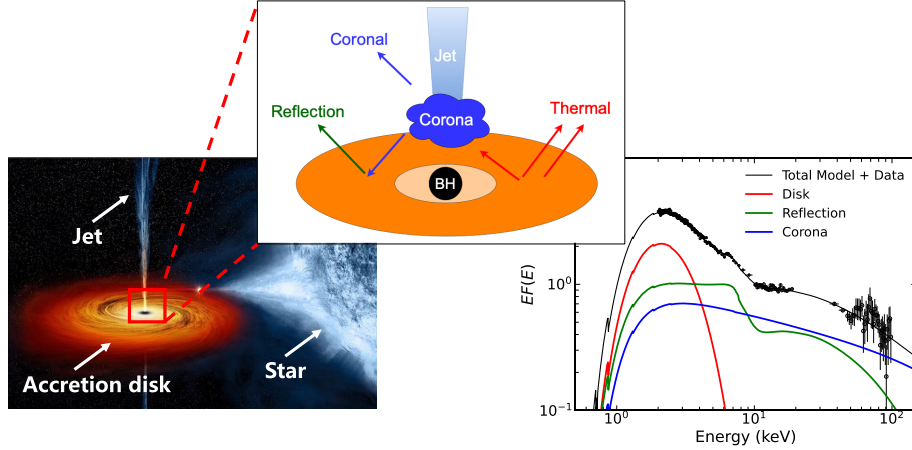


**Fig. 1** (Left) Artist’s impression of a black hole X-ray binary system (courtesy of JPL/NASA). (Middle) A zoom-in sketch of the inner accretion flow near a BH. Arrows with different colors represent emission components: (red) the disk thermal emission; (blue) the coronal emission; (green) the reflected emission of the disk. (Right) The Insight–HXMT observation of the low mass BH XRB GX 339–4 in the intermediate state on 2021 March 27. The red, blue and green lines show spectral components corresponding to the middle panel. The sum is shown as the black solid line. Figure adapted from Liu (2024).

timing variability. It is even possible to trace the outburst using timing properties only, such as the “hue angle” defined on the power spectral density (Heil et al., 2015). The hue angle is defined on a power-color (PC) diagram. Two power colors are first defined: (1) PC1: the variance in the 0.25–2.0 Hz band divided by the variance in the 0.0039–0.031 Hz band. (2) PC2: the variance in the 0.031–0.25 Hz band divided by the variance in the 2.0–16.0 Hz band. Observations have shown that during an outburst, the source traces an elliptical path on a PC2 versus PC1 diagram, centered at  $(PC1, PC2) = (4.5, 0.45)$  (see Figure 1 of Heil et al. 2015). The hue angle is then defined as the clockwise angle from a reference axis at  $45^\circ$  to the  $x$  and  $y$ -axes (see Figure 2 of Heil et al. 2015). The ranges of the hue angle corresponding to different spectral states are provided in Table 2 of Heil et al. 2015.

All of these different methods for characterising the time-evolving X-ray properties of a system reveal how a source transitions between distinct *states* during an outburst (e.g., Fender et al., 2004; Homan and Belloni, 2005; Remillard and McClintock, 2006). In Figure 3, the outbursts of three sources are shown to follow a similar pattern on the HID. As the source emerges from quiescence, it first enters the lower-right corner of the HID (region A), indicating a low luminosity and a hard X-ray spectrum. This is known as the *low hard* state during which the X-ray spectrum is dominated by a power-law-like component from the corona (see the right panel of Figure 3), and the radio emission indicates the presence of a steady compact jet (Corbel et al., 2003; Kylafis et al., 2012). As the accretion rate increases, the source moves upwards on the HID into the *bright hard* state (region B). During this phase, the source luminosity

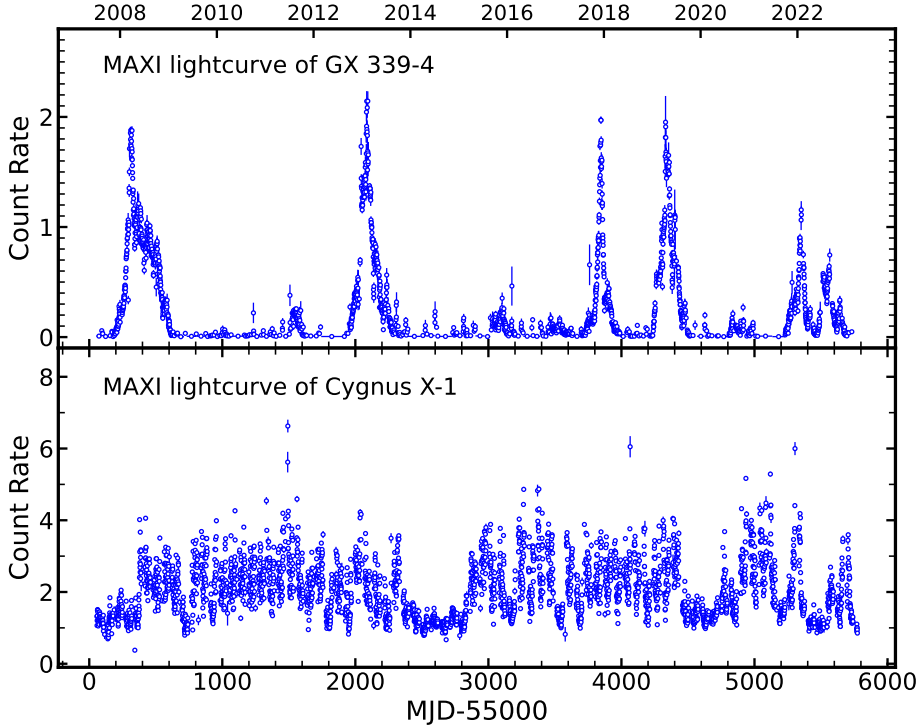


**Fig. 2** Lightcurves of a transient (GX 339-4) and a persistent (Cygnus X-1) BH XRBs by the Monitor of All-sky X-ray Image (MAXI) in the 2–20 keV band.

rises (as shown in Figure 3), while the spectral shape remains largely unchanged and continues to be dominated by the coronal component.

Then the source makes a leftward turn on the HID and transitions quickly to the *soft state* (region C), passing through the short-lived hard intermediate and soft intermediate states. The transition luminosity varies from source to source and may even differ between outbursts of the same source. The state transition is manifested as an increasing contribution from the disk thermal component and a steepening of the coronal component in the spectrum. During this transition, a highly relativistic, episodic, and ballistic jet is often launched (e.g., Körding et al., 2008; Bright et al., 2020), and the steady compact jet is then quenched (e.g., Russell et al., 2019). This roughly corresponds to the boundary between the hard and soft intermediate states (jet line in Figure 3, Fender et al. 2009; Miller-Jones et al. 2012; Homan et al. 2020).

In the soft state, thermal emission from the disk completely dominates the spectrum, while the coronal emission is diminished and the jet disappears. After spending most of the outburst time (weeks to months) in the soft state with steadily decreasing luminosity, the source transitions back to the low hard state (from region D to A) at a luminosity lower than that of the hard-to-soft transition. This “hysteresis effect” causes a “q”-shaped track on the HID. Since the intensity roughly corresponds to the mass accretion rate, the hysteresis implies that mass accretion rate alone does not

determine the spectral state and accretion flow properties (e.g., Meyer-Hofmeister et al., 2005; Liu et al., 2005; Petrucci et al., 2008; Begelman and Armitage, 2014). It should also be noted that some outbursts do not go through the whole q-diagram and finish without reaching the soft state (‘failed’ outbursts, Tetarenko et al., 2016; Alabarta et al., 2021; Wang et al., 2022b). Moreover, some peculiar individual sources do not exhibit a canonical q-diagram during their outbursts, though states can still be defined based on their spectral and timing properties (e.g., Belloni et al., 2000; Wijnands and van der Klis, 2000; Wang et al., 2024; Fan et al., 2024b).

Although persistent sources do not exhibit this kind of quiescence-outburst cycle, they still show strong variability in their lightcurves (see Figure 2). This variability can also be traced on the HID, where similar transitions between spectrally hard and soft states are observed (e.g., Smith et al., 2007; Hirsch et al., 2020; Jiang, 2024; König et al., 2024).

A common interpretation for the low hard state is that the accretion disk is truncated at a large radius (Tomsick et al., 2009), within which lies an optically thin, hot accretion flow that may act as the corona, producing strong power-law emission (Narayan and Yi, 1994; Done et al., 2007). In the high soft state, the accretion disk is thought to extend down to the innermost stable circular orbit (ISCO) (Steiner et al., 2010). However, significant debate remains regarding how the disk and corona evolve from the low hard to the high soft state, particularly through the bright hard and intermediate states. A key question is whether the disk remains truncated in the bright hard state, which has important implications for understanding the mechanism of state transitions.

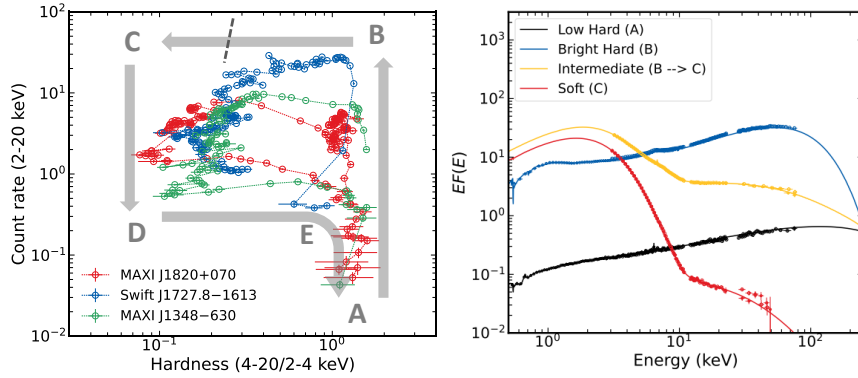


**Fig. 3** (Left) Hardness-intensity diagrams of three recent outbursts from transient BH XRBs plotted using MAXI data. The dashed line denotes the launch of ballistic jets. Figure adapted from Liu (2024). (Right) X-ray spectra of different states from *NuSTAR* and *NICER* observations of MAXI J1820+070.

## 3 X-ray techniques to measure accretion geometry

In this section, we summarize the X-ray techniques that can be used to measure/infer the geometry of the disk-corona system.

### 3.1 X-ray spectroscopy

X-ray spectroscopy involves the analysis of the X-ray spectra from sources, as shown in the right panels of Figure 1 and Figure 3.

#### 3.1.1 Spectroscopy of the Corona

For coronal geometries, a variety of models have been proposed in the literature, as summarized in Figure 1 of Poutanen et al. (2018). The basic geometry of the corona can be constrained from the shape of its spectrum. In the quiescent state, when the X-ray luminosity is very low (e.g.,  $L_X/L_{\text{Edd}} < 10^{-4}$ ), the photon index ( $\Gamma$ ) saturates at approximately 2.1 (Sobolewska et al., 2011; Plotkin et al., 2013; Reynolds et al., 2014). This is likely because the spectrum is dominated by jet emission, such as that from inverse Comptonization or synchrotron emission from a non-thermal particle distribution (Yuan and Cui, 2005). In the low hard state (region A of Figure 3), the coronal spectrum is hard (i.e., the photon index  $\Gamma \approx 1.6 - 1.8$ ) and its temperature is high ( $\sim 100$  keV). This is only possible in a “photon-starved” geometry, where the cooling power provided by seed photons (e.g. from the disk) is not too high. Otherwise, the corona would be cooled down and its spectrum would become soft. This constraint requires the ratio of the heating power in the corona ( $L_h$ ) to the power of the seed photons illuminating it ( $L_s$ ) to be:  $L_h/L_s \gg 1$ . In this case, the sandwich-corona (or slab-corona) geometry (Haardt and Maraschi, 1991, 1993), in which the corona fully covers the underlying cold disk, is ruled out. This is because half of the coronal emission is reprocessed by the disk and emerges as soft seed photons. This reprocessing forces  $L_h/L_s \sim 1$  and leads to a soft spectrum ( $\Gamma > 2$ ), even if all the accretion power is dissipated in the corona (Stern et al., 1995; Poutanen and Svensson, 1996; Malzac et al., 2001). Furthermore, intrinsic dissipation within the disk itself produces additional seed photons, resulting in even softer spectra.

There are alternative scenarios that meet the  $L_h/L_s \gg 1$  requirement:

- The truncated disk scenario, in which the standard geometrically thin, optically thick disk is truncated at a large radius. Inside this radius, a hot, geometrically thick, and optically thin accretion flow is present and provides the high-energy ‘coronal’ emission (Esin et al., 1997). This hot flow is generally believed to be an advection-dominated accretion flow (ADAF) (Ichimaru, 1977; Narayan and Yi, 1994). In this geometry, the hot flow intercepts only a small fraction of the soft photons from the outer disk.
- The patchy corona scenario, in which the corona consists of localized active regions on the surface of the disk (Haardt et al., 1994; Stern et al., 1995). Here, although half of the coronal emission is reprocessed by the disk, only a fraction of those reprocessed photons re-enter the corona as seed photons.

- The outflowing corona scenario, in which the corona moves away from the disk with a relativistic bulk velocity (Beloborodov, 1999; Malzac et al., 2001). In this case, beaming reduces the X-ray emission directed toward the disk, resulting in fewer reprocessed soft photons.

Among the three scenarios, the ADAF solution is only valid for low accretion rates (up to  $L/L_{\text{Edd}} \sim 0.01$  for a viscosity parameter  $\alpha = 0.1$ ; Esin et al. 1997). However, observations suggest the luminous hard state (Region B) can reach a much higher accretion rate ( $L/L_{\text{Edd}} \sim 0.2$ ; Gierliński and Done 2003; Koljonen et al. 2016; Liu et al. 2023a). The patchy-corona model naturally predicts comparable luminosities for the direct coronal emission and the reflection component, a prediction which contradicts observations in the fainter stages of the hard state (e.g., Cadolle Bel et al., 2007; Nowak et al., 2011; Fürst et al., 2015; Wang-Ji et al., 2018; Wang et al., 2020) but is consistent with data from the luminous hard state and intermediate states (e.g., Miller et al., 2002, 2004; Xu et al., 2018; Liu et al., 2023a). Ultimately, spectral fitting alone is often insufficient to distinguish between different coronal geometries (e.g., Brenneman et al., 2014) or to obtain detailed quantitative constraints on the corona.

### 3.1.2 Spectroscopy of the Disc

For the disk thermal emission component, the disk temperature increases as the disk moves closer to the black hole. In the meantime, relativistic effects (e.g., Doppler boosting and gravitational redshift) also become stronger because of the faster orbital velocities. Therefore, the disk thermal component can potentially be used to measure the inner disk radius. Practically, this can be done using the simple Newtonian model `diskbb` (Mitsuda et al., 1984) or more appropriate relativistic models such as `kerdd`<sup>2</sup> (Ebisawa et al., 2003) and `nkbb`<sup>3</sup> (Zhou et al., 2019). This method is most effective when the disk thermal component contributes significantly to the spectrum, such as during the intermediate and soft states. This technique is often referred to as *continuum fitting*. Using the continuum-fitting method alone to constrain the inner disk radius (or BH spin) requires prior knowledge of the BH mass, distance, and disk inclination angle<sup>4</sup> (Zhang et al., 1997; McClintock et al., 2014). This requirement limits the application of the method to sources where this information is known. One alternative is to implement continuum fitting together with the reflection method (see below). The reflection method can provide complementary constraints on the inner disk radius and disk inclination. Consequently, the priors on BH mass and distance can be relaxed, allowing these parameters to be measured using only X-ray data (e.g., Parker et al., 2016; Zdziarski et al., 2025; Das et al., 2025). Moreover, due to scattering in the disk atmosphere, the local emerging spectrum at a given disk radius often deviates from a true blackbody. This effect is typically modeled with a modified or diluted blackbody spectrum (Shimura and Takahara, 1995). The local specific flux is given by  $F_\nu = \pi B_\nu(f_{\text{col}} T_{\text{eff}}) / f_{\text{col}}^4$ , where  $f_{\text{col}}$  is the color correction factor,  $T_{\text{eff}}$  is the

<sup>2</sup><https://heasarc.gsfc.nasa.gov/xanadu/xspec/manual/node190.html>

<sup>3</sup><https://github.com/ABHModels/nkbb>

<sup>4</sup>It has been shown via simulations that high-quality X-ray spectra allow the continuum-fitting method to simultaneously constrain the black hole spin and the inclination of the disk. This requires a well measured thermal disk emission across a wide energy range (Parker et al., 2019).

local effective temperature, and  $B_\nu$  is the Planck function. The color correction factor is often assumed to be constant, i.e., independent of disk radius and accretion rate, in spectral fitting. Such an assumption is likely appropriate within a single observation. Simulation work has suggested a canonical value of 1.7 for the color correction factor (Shimura and Takahara, 1995; Davis et al., 2005). However, in principle, this factor should vary with spectral state and accretion rate (e.g., Merloni et al., 2000; Ren et al., 2022).

### 3.1.3 Reflection Spectroscopy

Analysis of the reflection component is also a powerful tool for studying the accretion geometry. As shown in Figure 4, the reflection spectrum in the local rest frame of the disk is characterized by fluorescent emission lines (the strongest one being the iron  $K\alpha$  line), photoelectric absorption edges and a Compton reflection hump peaking around 30 keV (George and Fabian, 1991; García and Kallman, 2010). The commonly used local reflection models are `reflionx`<sup>5</sup> (Ross and Fabian, 2005) and `xillver` (García and Kallman, 2010). These models calculate the reflection spectrum of an ionized disk. There are also models specifically for neutral disks, such as `pexrav`<sup>6</sup> (Magdziarz and Zdziarski, 1995) and `pexmon`<sup>7</sup> (Nandra et al., 2007).

The local reflection spectrum, resulting from irradiation of the disk by the corona, will be altered by several relativistic effects, including Doppler shifts, gravitational redshift, and light bending. The left panel of Figure 4 illustrates how a narrow line at 6.4 keV becomes broadened and skewed due to these effects from the accretion disk when integrated over the whole profile of the disk. A detailed discussion of how various system parameters (e.g., inner disk radius, disk inclination angle, etc.) impact the broad line profile can be found in Fabian et al. (2000) and Gates et al. (2024). The red wing of the broadened profile extends to lower energy as the inner disk radius decreases, making it a useful probe of disk geometry. Additionally, the emissivity profile, namely the radial dependence of the reflected emission intensity, is determined by the coronal geometry (e.g., Wilkins and Fabian, 2011, 2012), though it can be challenging to reconstruct the corona geometry directly from the observed phenomenological emissivity profile. Several models exist to compute relativistic line broadening, including `diskline` (Fabian et al., 1989) `laor` (Laor, 1991), `kyrline` (Dovčiak et al., 2004), `kerrdisk` (Brenneman and Reynolds, 2006) and `relline` (Dauser et al., 2010).

Applying the broadening kernel to the local reflection spectrum yields the relativistic reflection model (e.g., Bambi, 2024a), which can be used to fit observational data and infer the disk-corona geometry. A summary of available reflection models and possible source of systematic uncertainties can be found in Bambi et al. (2021). The two main features of the resulting relativistic reflection spectrum seen by an external observer are the broad iron line around 6.4 keV and the Compton hump peaked around 30 keV. These features have been commonly found in the hard and intermediate states of BH XRBs (e.g., Walton et al., 2016; Jiang et al., 2019; Liu et al., 2023a,b).

---

<sup>5</sup><https://github.com/honghui-liu/reflionx-tables>

<sup>6</sup><https://heasarc.gsfc.nasa.gov/xanadu/xspec/manual/node214.html>

<sup>7</sup><https://heasarc.gsfc.nasa.gov/xanadu/xspec/manual/node213.html>

X-ray reflection models have been significantly developed over the past 15 years. However, like all models, they rely on several simplifications. These can introduce systematic uncertainties into parameter estimation, in addition to statistical uncertainties. The key simplifications can be classified into the following categories:

- ***Simplifications in disk geometry assumptions.*** The accretion disk is often modeled as an infinitesimally thin Keplerian disk aligned perpendicularly to the black hole spin axis. However, a realistic disk has a finite thickness (Taylor and Reynolds, 2018). The impact of this thin-disk assumption on black hole spin measurements (thus  $R_{\text{in}}$ ) is marginal in the sub-Eddington regime (e.g.,  $L/L_{\text{Edd}} < 0.3$ ; Abdikamalov et al. 2020; Tripathi et al. 2021; Jiang et al. 2022). In the near-Eddington regime, radiation pressure causes vertical expansion of the disk, resulting in a thick-disk geometry rather than a thin one. Simulations have shown that applying the thin-disk assumption under these conditions can lead to significant biases in the estimation of key parameters like BH spin (Taylor and Reynolds, 2018; Riaz et al., 2020a,b). In the super-Eddington regime, strong, optically thick outflows with relativistic velocities and large opening angles become the primary component responsible for reflecting the coronal emission (Thomsen et al., 2019). Consequently, line broadening is dominated by the kinematics of the wind and its opening angle (Zhang et al., 2024). Therefore, the thin-disk assumption must be significantly modified to fit observational data in this regime (e.g., Shashank et al., 2024).
- ***Simplifications in coronal geometry assumptions.*** The coronal geometry determines the emissivity profile of the disk reflection component (Wilkins and Fabian, 2012), but it remains poorly constrained. Simple geometries, such as the lamppost model where the corona is approximated as a point source located at a certain height above the black hole, have been used to construct reflection models (Dauser et al., 2013). However, a realistic corona must have a radial extension to efficiently intercept seed photons from the disk. Therefore, models implementing a disk-like or ring-like corona above the BH have also been developed (Riaz et al., 2022). The ring-like coronal model has been applied to an AGN system and described the data well (Nekrasov et al., 2025). They found that the corona should be compact, with both its vertical and radial extents being less than  $\sim 3 R_g$ . This is in agreement with what is implied by fitting the data using a simple lamppost model. Such a test proves the concept of developing and applying more realistic coronal geometries for X-ray data. Alternatively, it is common to model the emissivity profile directly using phenomenological models, such as a power-law or broken power-law. In practice, it is recommended to test different geometries during spectral fitting to check for model dependence in the results.
- ***Simplifications in the calculation of local reflection spectrum.*** Current reflection models are calculated assuming a parallel-slab configuration with a constant density in the vertical direction. This constant-density assumption might be appropriate in the radiation pressure-dominated regime. However, the accretion disk in the hard state of BH XRBs is expected to be gas pressure-dominated, a condition that naturally predicts a vertically stratified density structure, with higher density towards the disk mid-plane. Evidence for such structure has been presented by Liu et al. (2023b), who found that the densities measured at the disk surface in

the hard state of BH XRBs are lower than the theoretical predictions for the disk center. Local reflection spectra have been calculated for a gaussian density profile (Ballantyne et al., 2001) or a density profile from hydrostatic equilibrium (Nayakshin et al., 2000). However, a full model that can be tested on data is still lacking. Moreover, most currently employed reflection models often assume no upward radiation flux at the bottom boundary. This is appropriate for AGN disks, which are relatively cold. In contrast, disks in XRBs can be significantly hotter, with temperatures reaching 1–2 keV in the soft and intermediate states. This intrinsic thermal emission can therefore influence the ionization structure of the disk. The impact of a hot disk has been incorporated in the `reflionx` model (Ross and Fabian, 2007) and studied in specific sources (Reis et al., 2008, 2009, 2011, 2012; Steiner et al., 2011, 2012b; Walton et al., 2012; Chiang et al., 2012; Reis et al., 2013; King et al., 2014; Xu et al., 2020b). A test of the model by Liu et al. (2023a) found no strong impact on the measurement of  $R_{\text{in}}$ . A caveat even with these studies, however, is the assumption of a single-temperature blackbody spectrum for the disk. In reality, an accretion disk emits a multi-temperature blackbody spectrum, with higher temperatures at smaller radii. This radial temperature gradient will inevitably lead to a radius-dependent ionization state.

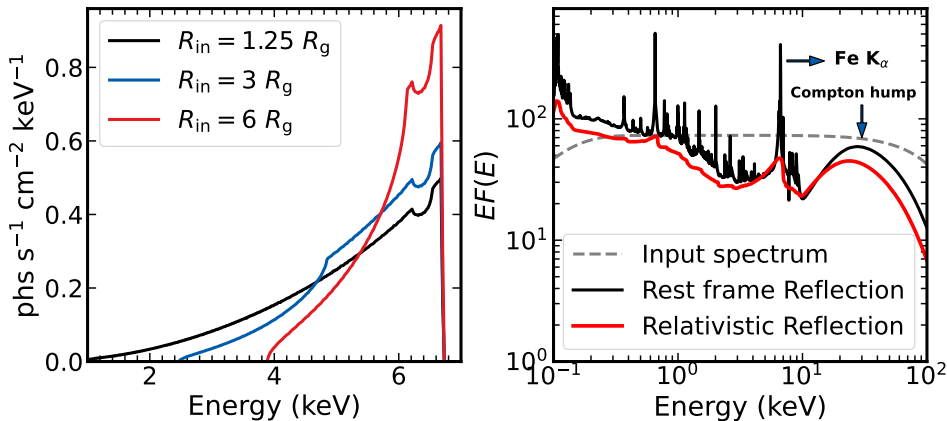


**Fig. 4** (Left) The broad iron line profiles as a function of the inner disk radius ( $R_{\text{in}}$ ). The profiles are calculated using the `relline` model assuming a black spin  $a_* = 0.998$ , an inclination angle  $i = 30^\circ$ , an power-law emissivity profile with the index  $q = 3$  and an outer disk radius  $R_{\text{out}} = 400 R_g$ . (Right) Rest-frame reflection (black) and relativistic reflection (red) spectra for an accretion disk extending to the innermost circular orbit.

### 3.2 X-ray timing

The accretion flow is highly dynamic, exhibiting X-ray variability on timescales ranging from milliseconds to years. Timing analysis mainly operates in the frequency domain. One of the main timing products is the power spectral density (PSD), which shows the variability power as a function of frequency (van der Klis, 1989; Uttley et al., 2014).

In the hard and intermediate states, the PSD often shows narrow peak features known as quasi-periodic oscillations (QPOs), indicating enhanced variability at characteristic frequencies (Motta et al., 2011; Ingram and Motta, 2019; Liu et al., 2021). The QPO frequencies may be linked to dynamic processes in the system (e.g., Lense-Thirring precession, Ingram et al. 2009) or to oscillation modes of the accretion flow (Tagger and Pellat, 1999; Varnière and Tagger, 2002; Chakrabarti et al., 2008; Varnière et al., 2012). Therefore, they may potentially provide insights into the accretion geometry or fundamental parameters such as the black hole mass and spin (e.g., Motta et al., 2014).

Other important timing products are the lag-frequency spectrum (e.g., the phase lag between lightcurves of two energy bands) and the lag-energy spectrum (phase lag relative to a reference energy band in a specific frequency range). A typical lag-frequency spectrum (0.5–1.0 v.s. 1.0–10.0 keV) for a BH XRB is shown in the left panel of Figure 5. There is strong contribution from the reflection component in the soft band and the hard band is dominated by the coronal emission. A hard/positive lag (i.e., hard photons lagging behind soft photons) is observed at low frequencies (0.1–1.0 Hz), and is thought to originate from mass accretion rate fluctuations propagating through the accretion disk (Lyubarskii, 1997; Ingram and Done, 2011, 2012). In the lag-energy spectrum at low frequencies, the lag continues to rise with energy (the *continuum lag*, see the right panel of Figure 5). In this spectrum, one should focus on the relative shape because the absolute lag values depend on the choice of the reference band. The lag-energy spectrum should be interpreted from bottom to top; that is, a smaller lag indicates that the signal arrives earlier at the detector. The steadily increasing trend with energy implies that high-energy X-ray photons always lag behind low-energy photons when low-frequency variations are considered. At high frequencies, the *reverberation lag*, which has a more complex structure, starts to dominate. This lag arises because the reflection component responds to variability in the coronal emission with a delay due to light-travel time (e.g. Zhan et al., 2025). Consequently, the lag-energy spectrum at high frequencies resembles the shape of the reflected energy spectrum (see the lower panel of Figure 5).

It is evident that the tool can be applied to both XRB and AGN systems. However, most reverberation mapping studies over the past two decades have focused on AGNs (Fabian et al., 2009; Zoghbi et al., 2012, 2014; Kara et al., 2015, 2016; Mastroserio et al., 2020), as detecting reverberation in XRBs is more challenging due to their smaller lag amplitudes and higher frequency ranges. A comparison of lag properties between XRBs and AGNs can be seen in Figure 7 of Kara and García (2025), which illustrates how the lag amplitude scales with BH mass and how the reverberation-dominated frequencies scale inversely with it.

One commonly used model for analyzing reverberation lags is `reltrans`<sup>8</sup> (Ingram et al., 2019), which can simultaneously fit the reflection spectrum. The model assumes a lamppost geometry for the corona and can constrain its height using both spectral and timing information. Another important model in the literature is `vkompth`<sup>9</sup> (Bellavita et al., 2022), which is primarily designed for the study of QPOs and fits

---

<sup>8</sup><https://github.com/reltrans>

<sup>9</sup><https://github.com/candebellavita/vkompth>

the energy-dependent rms-amplitude and phase-lag spectra at the QPO frequency to estimate the size of a spherical corona. One strength of the `vKompth` model is that it can fit the time-averaged Comptonization spectrum simultaneously with the lag and rms spectra. This model attributes the hard lag to the Comptonization process, where higher-energy photons require more scatterings within the corona. Note that this is a different assumption from the fluctuation-propagation scenario. The soft lag is attributed to the feedback and reprocessing of coronal photons in the disk, which is treated as thermalization into a blackbody spectrum. The relative importance of these two processes is controlled by the feedback parameter, defined as the fraction of the disk thermal emission that originates from reprocessed coronal emission. This parameter can be converted into the “intrinsic feedback”, which is the fraction of the coronal emission that returns to the disk.

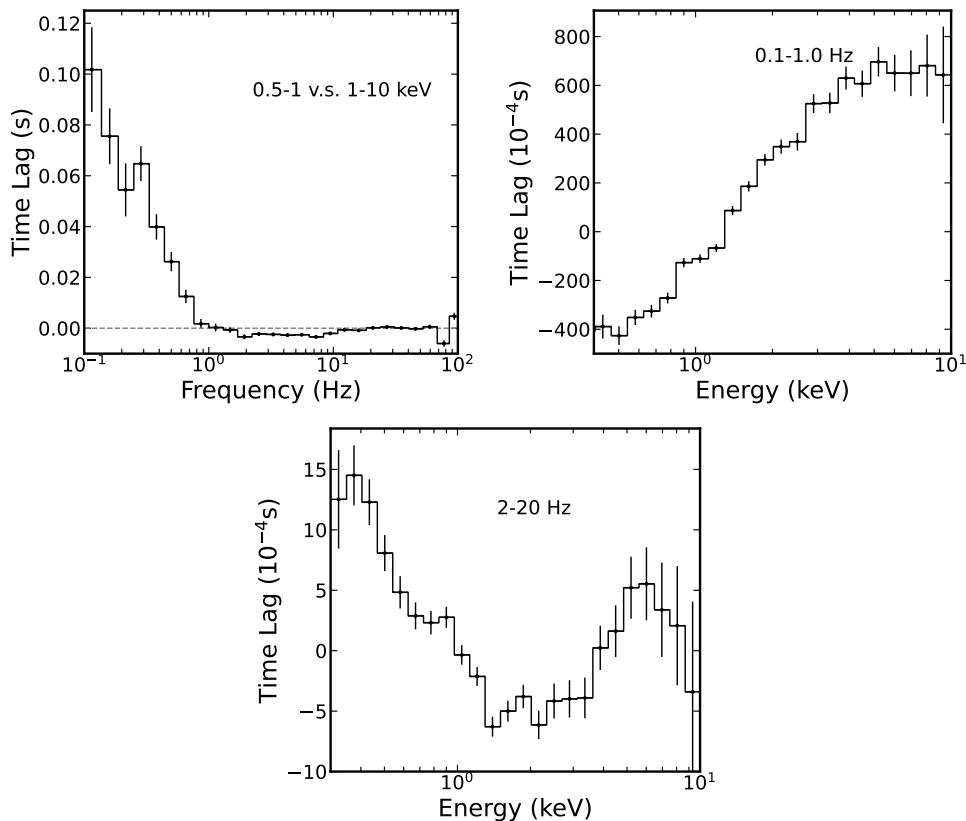


**Fig. 5** (Upper Left) Lag-frequency spectrum between the 0.5–1 keV and 1–10 keV bands for the black hole X-ray binary MAXI J1820+070 from a NICER observation. (Upper Right) Lag-energy spectrum from the same data in the 0.1–1.0 Hz frequency range, using the 0.5–10 keV band as a reference. (Lower) Lag-energy spectrum in the 2–20 Hz frequency range.

### 3.3 X-ray Polarimetry

The measurement of X-ray polarization properties, i.e., the polarization degree (PD) and polarization angle (PA), offers strong potential for probing the details of the disk-corona geometry. These two parameters represent how electric field vectors of X-ray photons are preferentially distributed along a specific orientation. They are sensitive to the geometry of the emission region and the underlying emission mechanism.

In the case of the thermally Comptonized emission, a higher PD is expected in more asymmetric systems, while the PA indicates the orientation of the Comptonizing medium (Schnittman and Krolik, 2010). The PD, PA, and their energy dependence for a given coronal geometry can be calculated using Monte Carlo-based codes such as MONK (Zhang et al., 2019) and KerrC (Krawczynski and Beheshtipour, 2022). These codes can also provide the simultaneous energy spectrum of the corona. However, it can be computationally expensive to construct a grid of models to fit spectropolarimetric data. Alternatively, for a slab geometry, these polarimetric properties can be calculated using a radiation transport solver such as COMPPS (Poutanen and Svensson, 1996; Veledina and Poutanen, 2022).

The thermal emission from an optically thick accretion disk is expected to be polarized parallel to the disk plane, with a PD that depends on the inclination angle (Chandrasekhar, 1960). When considering scattering as the only relevant process, the polarization properties of a disk with finite optical depth can be calculated using the Monte Carlo code STOKES<sup>10</sup> (Goosmann and Gaskell, 2007; Marin, 2018). Since the disk geometry can be approximated as a slab, its polarimetric properties for various optical depths can be pre-calculated and tabulated efficiently. A more self-consistent treatment should consider other processes such as absorption. This can be achieved by combining the STOKES code with a radiative transfer and photoionization code that can calculate the ionization structure of the disk surface (e.g., Taverna et al., 2021). General relativistic (GR) effects are also crucial, as polarization vectors rotate due to parallel transport along null geodesics. This effect is more significant for larger BH spins, offering an alternative method for constraining the spin parameter (Dovčiak et al., 2008). Spectro-polarimetric models for disk thermal emission that incorporate these effects have been developed, such as KYNBB (Dovčiak et al., 2008) and KYNBBRR (Taverna et al., 2020). The latter model additionally accounts for the returning radiation effect, whereby photons emitted from the disk are bent by the strong gravitational field and fall back onto the disk.

The reflection component also has distinct polarization signatures, including a highly polarized continuum and depolarized fluorescent lines (Matt, 1993; Podgorný et al., 2022, 2023). The exact polarization spectrum depends on the coronal geometry and its polarimetric properties, the ionization state of the disk, the inclination angle, and the black hole spin. A spectro-polarimetric model, KYNSTOKES (Podgorný et al., 2023), has been developed to account for these effects. In this model, the spectral and polarimetric properties of the local disk reflection are calculated by combining the radiative transfer code TITAN (Dumont et al., 2003) with the STOKES code. General

---

<sup>10</sup>The STOKES code is available at: [https://people.astro.unistra.fr/marinf/STOKES\\_web/index.html](https://people.astro.unistra.fr/marinf/STOKES_web/index.html). Pre-calculated polarimetric tables for disk thermal emission can be downloaded from: <https://projects.asu.cas.cz/stronggravity/kyn#kynbb>.

relativistic effects are subsequently incorporated using the KY package (Dovčiak et al., 2004, 2011).

High sensitivity X-ray polarimetry measurements have only been possible since the launch of the Imaging X-ray Polarimetry Explorer (IXPE) on 9 December 2021 Weisskopf et al. (2022). IXPE, operating in the 2–8 keV band, has observed a dozen BH XRBs, yielding significant breakthroughs in the understanding of the disk-corona geometry (see Dovčiak et al., 2024, for a recent review).

## 4 Accretion geometry inferred from X-ray observations

As our main vehicle for summarising our current understanding of the evolving accretion geometry in BH XRBs, a compilation of inner disk radius ( $R_{\text{in}}$ ) measurements from pile-up<sup>11</sup> free data is shown in Figure 6. We select sources that meet the following three criteria: (1) Available distance and BH mass measurements to compute the Eddington limit. (2) Eddington ratio measurements (e.g.,  $L_X/L_{\text{Edd}}$ ) published alongside the  $R_{\text{in}}$  measurements using relativistic models. (3) Data obtained from pile-up free instruments, such as *RXTE*, *Insight-HXMT*, *NuSTAR*, and *NICER*, in the hard and intermediate states. Basic information about the sources can be found in Table 1. In cases where the same observation has been analyzed multiple times in the literature, we include only the most recent measurement of  $R_{\text{in}}$ . These measurements are derived from X-ray spectroscopy, as current X-ray timing and polarimetry data are not yet capable of reliably constraining the  $R_{\text{in}}$  parameter for XRBs. The  $R_{\text{in}}$  measurements in Figure 6 are predominantly obtained via the reflection method. A notable exception is MAXI J1820+070, where the values are derived from a combination of continuum fitting and reflection (Fan et al., 2024a) (excluding the two lowest-luminosity points from Xu et al. 2020a). We will discuss the accretion geometry based on Figure 6, incorporating relevant insights from X-ray timing and polarimetry measurements.

### 4.1 Hard state (Region A to B)

This region corresponds to the right branch of the HID and represents the emergence from quiescence and the evolution from the low hard (region A of Figure 3) to the bright hard (B) states. Figure 6 shows that at the beginning and end of the outburst (region A), when the accretion rate is low ( $L_X/L_{\text{Edd}} \sim 0.1\%$ )<sup>12</sup>,  $R_{\text{in}}$  is truncated at large radii (e.g.,  $> 100 R_{\text{ISCO}}$ ). As the accretion rate increases, the disk moves closer to the BH, but typically remains truncated at  $\sim 10 R_g$  if  $L_X/L_{\text{Edd}} < 1\text{--}2\%$ . In this regime, a hot inner flow likely exists between the inner edge of the disk and the BH, acting as the corona. This radially extended coronal geometry in the low-hard state is consistent with IXPE measurements of Cygnus X-1 (taken at  $L_X/L_{\text{Edd}} \sim 1\%$ , Krawczynski et al., 2022) and Swift J1727.8–1613 (taken at  $L_X/L_{\text{Edd}} \sim 0.5\%$ , Podgorný et al., 2024). In both cases, the PA of the coronal emission was found to align with the radio jet

<sup>11</sup>Pile-up is an effect where two or more photons hit the same pixel (or neighboring pixels) during a single readout frame. The detector will incorrectly register them as one single event, distorting the observed X-ray spectrum.

<sup>12</sup> $L_{\text{Edd}}$  is the Eddington luminosity defined as  $L_{\text{Edd}} = 1.26 \times 10^{38} M_{\text{BH}}/M_{\odot} \text{ erg s}^{-1}$ .

direction, suggesting a radially extended corona (i.e. extended in the disk plane). *IXPE* measurements also rule out the lamppost and spherical lamppost coronal geometries, as they produce a PD that is too low compared to the observed values (Ursini et al., 2022; Krawczynski et al., 2022). The decreasing trend of  $R_{\text{in}}$  with luminosity along the right branch is also consistent with the X-ray reverberation measurements. For instance, Wang et al. (2022a) found that the reverberation lag amplitude in eight BH XRBs decreases along the right branch (see their Figure 6), which would naturally result from the disk moving inward toward the BH and the corona contracting radially.

As the accretion rate continues to increase,  $R_{\text{in}}$  can reach the ISCO even in the hard state when  $L_X/L_{\text{Edd}} > 3\text{--}4\%$ . Among all the hard-state measurements in Figure 6 with  $L_X/L_{\text{Edd}} > 3\%$  (23 in total), 78% (18/23) are consistent with  $R_{\text{in}} < 4 R_{\text{ISCO}}$ , and 43% (10/23) are consistent with  $R_{\text{in}} < 2 R_{\text{ISCO}}$  (including three upper limits). These findings indicate that *the accretion disk is not necessarily truncated in the bright hard state*. The geometric evolution of the disk-corona system already takes place in the hard state and is not limited to the state transition. This is not surprising given that the source luminosity varies by orders of magnitude during this phase.

An interesting finding is that even when the disk reaches (and remains at) the ISCO during the bright hard state (region B), the reverberation lag amplitude continues to decrease and the upper bound of the soft lag frequency<sup>13</sup> tends to increase with time (see Kara et al., 2019; Wang et al., 2022a). Since the inner radius of the disk is stable in this region, the decreasing lag and increasing frequency are interpreted as the corona shrinking in the vertical direction. This scenario is further supported by spectral fitting of the *NuSTAR* data of MAXI J1820+070 using a dual-lamppost model (Buisson et al., 2019), which can mimic a vertically extended corona (Lucchini et al., 2023).

There are hints that indicate a connection between the corona and the jet. It has been suggested that the base of the jet could produce the Comptonized emission (Markoff et al., 2005; Cao et al., 2022). In the bright hard state of MAXI J1820+070, the reflection strength has been found to decrease with time while the iron line profile remains stable. The stable line profile indicates a constant inner disk radius. This decreasing reflection strength has been interpreted with a scenario involving a jet-like corona whose bulk velocity increases with time (You et al., 2021). In the same MAXI J1820+070 data, Ma et al. (2021) detected low-frequency QPOs above 200 keV. They also discovered a long soft lag ( $\sim 0.9$  s) at the QPO frequency between 150–200 keV photons and those below 30 keV. This was interpreted within a precessing jet scenario, where high-energy photons originate from the jet base and low-energy photons from farther out in the jet. The jet’s precession produces the QPO, and a soft lag would naturally arise if the jet base is observed before the downstream emission region. Notably, the outflowing corona scenario has also been invoked to explain the higher-than-expected PDs observed in *IXPE* observations of several BH XRBs (Krawczynski et al., 2022; Poutanen et al., 2023; Ratheesh et al., 2024; Ewing et al., 2025). In the hard state of Cygnus X-1, *IXPE* measured a PD  $\sim 4\%$ , which is higher than the expected PD of 1% given the orbital inclination of the system

---

<sup>13</sup>This is the frequency ( $f_0$ ) at which the lag-frequency spectrum crosses zero. The lag flips into positive at this frequency due to phase wrapping. Therefore, this frequency is related to the intrinsic time delay ( $\tau$ ) between the coronal and reflected photons in a way:  $f_0 \sim 1/2\tau$

**Table 1** Selected sources with distance, mass, and inclination measurements.

Source	Distance (kpc)	Mass ( $M_{\odot}$ )	Inclination ( $^{\circ}$ )	Ref
GRS 1716–249	$6.9 \pm 1.1$	$6.4^{+3.2}_{-2.0}$	$61 \pm 15$ (binary)	1
GRS 1739–278	6–8.5	4.0–9.5	-	2,3
GX 339–4	8–12	4–11	40–60 (binary)	4
H 1743–322	$8.5 \pm 0.8$	$12 \pm 2$	$75 \pm 3$ (jet)	5,6
IGR J17091–3624	11–17	8.7–15.6	-	7,8
MAXI J1348–630	$3.39 \pm 0.38$	$11 \pm 2$	-	9
MAXI J1820+070	$2.96 \pm 0.33$	$9.2 \pm 1.3$	$63 \pm 3$ (jet)	10
MAXI J1535–571	$4.1^{+0.6}_{-0.5}$	$10.4 \pm 0.6$	-	11,12

*Note.* Selected sources and their properties. For references about the measurements of the distance, mass and inclination angle: (1) Casares et al. (2023); (2) Greiner et al. (1996); (3) Wang et al. (2018); (4) Zdziarski et al. (2019); (5) Steiner et al. (2012a); (6) Nathan et al. (2024); (7) Rodriguez et al. (2011); (8) Iyer et al. (2015); (9) Lamer et al. (2021); (10) Atri et al. (2020); (11) Chauhan et al. (2019); (12) Sridhar et al. (2019)

(Krawczynski and Beheshtipour, 2022). Similarly, a high PD of 9% was found in the hard state of IGR J17091–3624, which is high even for a high-inclination system (Ewing et al., 2025). An outflowing corona with a non-zero bulk velocity could increase the PD due to relativistic aberration (Poutanen et al., 2023), offering a potential explanation for these high polarization measurements. For Cygnus X-1, an alternative explanation for the high observed PD is that the corona is more inclined than the binary system, i.e., a warped disk. Such a configuration is possible if the orbital angular momentum is not aligned with the BH spin (Bardeen and Petterson, 1975).

## 4.2 Intermediate states (Region B to C)

This region corresponds to the upper branch of the HID and marks the hard-to-soft state transition. Since the accretion disk already extends close to the ISCO radius before the transition (i.e., during the bright hard state), we expect  $R_{\text{in}}$  to remain near  $R_{\text{ISCO}}$  throughout the state transition. Monitoring the transition process is challenging, as the starting point is unpredictable, and the transition timescale is short. The best-monitored source is GX 339–4, for which hard-to-soft transitions have been captured multiple times by *RXTE* (Sridhar et al., 2020) and *Insight-HXMT* (Liu et al., 2023a). The spectroscopic data from GX 339–4 indeed suggest that  $R_{\text{in}}$  remains stable and close to  $R_{\text{ISCO}}$  during the state transition (see empty symbols in Figure 6). Spectroscopic studies of other sources have also confirmed this behavior (e.g., Tao et al., 2019; Draghis et al., 2020; Wang et al., 2021; Ren et al., 2022; Fan et al., 2024a; Adegoke et al., 2024). Notably, the disk temperature at  $R_{\text{in}}$  continues to increase toward the soft state (Liu et al., 2023a), which could provide stronger cooling to the corona.

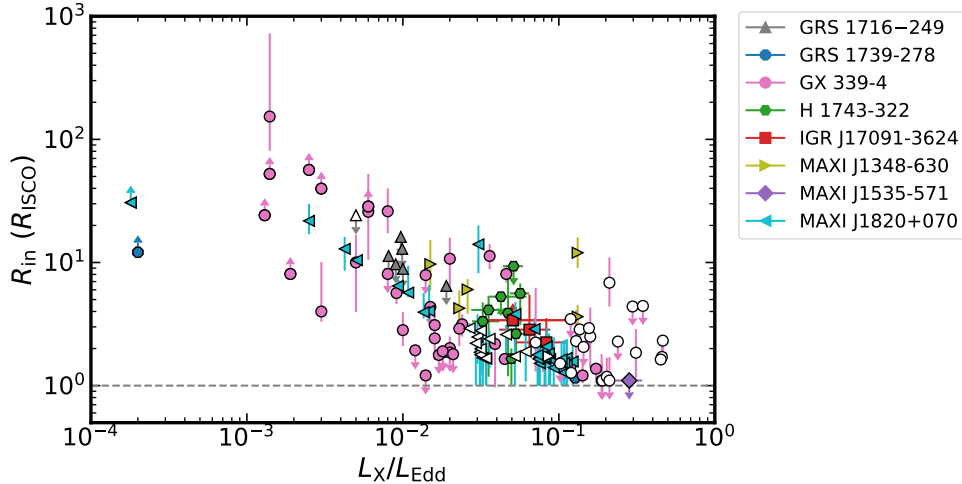


**Fig. 6** The evolution of the inner disk radius ( $R_{\text{in}}$ ) with the Eddington-scaled luminosity. The measurements of  $R_{\text{in}}$  are from X-ray spectroscopy. The filled symbols represent hard state data and the empty symbols are for intermediate states. Information of the selected sources can be found in Table 1.

**(References)** GX 339-4: Reis et al. (2008), Tomsick et al. (2008), Tomsick et al. (2009), Shidatsu et al. (2011), Petrucci et al. (2014), García et al. (2015), Wang-Ji et al. (2018), García et al. (2019), Sridhar et al. (2020), Wang et al. (2020), Liu et al. (2023a); GRS 1739-278: Furst et al. (2016), Liu et al. (2023b); GRS 1716-249: Jiang et al. (2020); MAXI J1348-630: Jia et al. (2022); IGR J17091-3624, H 1743-322, MAXI J1535-571: Liu et al. (2023b) and MAXI J1820+070: Xu et al. (2020a), Fan et al. (2024a).

Spectroscopic studies can suffer from degeneracies. Such degeneracies prevent us from placing strong constraints on the geometry and dynamics of the corona. However, combining spectroscopy with timing techniques can yield additional insights. From the soft lag sample compiled by Wang et al. (2022a), it was found that — unlike the decreasing trend in the hard state — the soft lag amplitude tends to increase during the hard-to-soft transition. Fitting the lag spectra with the `reltrans` model further suggests that the corona height increases along with the transition (Wang et al., 2021; DeMarco et al., 2021), indicating a vertical expansion of the corona that may be related to the transient jet ejections (e.g., Davidson et al., 2025). Similar corona-jet connections have also been inferred from correlations between radio flux and disk-corona parameters (e.g., Vadawale et al., 2003; Méndez et al., 2022). Moreover, X-ray flaring associated with transient jet activity has been found in a few BH XRBs (Punsly and Rodriguez, 2013; Walton et al., 2017). In V404 Cyg, the jet itself appears to have temporarily acted as the X-ray source that illuminates the disk (Walton et al., 2017).

Note that an alternative explanation for the soft lag in the intermediate states has been proposed by Kawamura et al. (2023) within the framework of mass accretion rate fluctuations. Typically, fluctuation propagation produces hard lags, as fluctuations from larger radii (emitting softer radiation) modulate the harder emission originating from smaller radii in a radially stratified corona. However, soft lags can also be produced if the hard Comptonization spectrum extends to lower energies than the soft Comptonization spectrum. This condition can be achieved if the seed photons for the

central Comptonization region are much cooler than those from the inner disk edge that provide seed photons for the outer Comptonization region. Another potentially important effect is the thermalization/scattering time delay within the reflection process (Salvesen, 2022). This effect is more significant for softer emerging photons, as they must undergo numerous scatterings to thermalize before escaping the disk. Current reverberation models assume instantaneous reprocessing; however, the scattering time delay may be longer than the light-travel time delay in the intermediate states (Salvesen, 2022).

While the `reltrans` model does not apply to the lags at the QPO frequency, the `vKompth` model is specifically designed to interpret lag and RMS spectra associated with QPOs. This model has been applied to several sources, and the feedback parameter has been observed to decrease during the state transition compared to the hard state (e.g., García et al., 2021, 2022a; Zhang et al., 2022, 2023; Ma et al., 2023; Peirano et al., 2023). Since this parameter represents the coupling strength between the disk and the corona, its decrease suggests that the corona evolves from a strongly coupled configuration (e.g., horizontally extended) to a weakly coupled one (e.g., vertically extended). However, it is important to note that the model inherently assumes a spherical coronal geometry. Therefore, this should be regarded as an empirical interpretation of the geometry, based on the data rather than a prediction of the model. In addition, the coronal sizes inferred from this model are generally large (hundreds of  $R_g$ ). In some cases, a two-corona scenario has been proposed to fully explain the QPO lag and rms spectra (Peirano et al., 2023), in which the smaller corona is found to have a size of tens of  $R_g$  (e.g., Ma et al., 2023; Alabarta et al., 2025). A spherical corona with a size of hundreds of  $R_g$  would be difficult to reconcile with constraints obtained from other methods. X-ray reverberation analyses of AGNs suggest that the corona is compact ( $\sim 10 R_g$ , Emmanoulopoulos et al. 2014). Measurements from microlensing studies also indicate that the X-ray-emitting region in luminous AGNs has a size smaller than  $10 R_g$  (Dai et al., 2010). We expect a similar coronal size in BH XRBs, as these systems are essentially mass-scaled-down versions of AGNs (McHardy et al., 2006; Reis and Miller, 2013). Future model developments that consider alternative geometries, such as vertically extended or jet-like coronae, and more physical processes, such as the propagation of heating within the corona, may help to deliver a more consistent picture.

X-ray polarization measurements in this branch have been conducted during the hard-intermediate state, e.g., before the launch of discrete jets, of Swift J1727.8–1613 (Veledina et al., 2023; Ingram et al., 2024) and in the soft-intermediate of GX 339–4 (Mastroserio et al., 2025). In these observations, the PA is found to align with the jet direction, similar to the low-hard state. This may suggest that the corona is horizontally extended along the accretion disk plane, which appears to conflict with the vertically extended geometry implied by reverberation lag measurements and the small inner disk radius inferred from spectroscopic studies. The latter conflict might be alleviated if the disk and corona are not radially separated, e.g., if the corona overlaps the disk (see Figure 7 and discussions in Liu and Qiao 2022). The dual-corona structure proposed by Peirano et al. (2023), in which a horizontally extended corona dominates

the spectral shape while a vertically extended corona dominates the lag, could potentially reconcile the former conflict. An illustration of such a dual-corona configuration is shown in the upper region of Figure 7. However, it should be noted that alternative scenarios also exist to explain the X-ray polarization measurements. For example, scattering off the walls of a jet could produce a PA aligned with the jet without requiring a horizontally extended corona (Dexter and Begelman, 2024). Alternatively, optically thin synchrotron emission from the jet could generate a similar PA, although its overall impact depends on its flux contribution to the IXPE band, the viewing angle, and the magnetic field structure (Russell and Shahbaz, 2014). This emission can be highly polarized (up to 70%) and has already been detected in Swift J1727.8–1613 at gamma ray energies (Bouchet et al., 2024). Lastly, such a PA could also arise from the returning radiation effect (i.e., photons emitted from the disk that return to the disk) due to the strong gravitational field near BHs (e.g., Steiner et al., 2024), or from scattering by disk winds (e.g., Nitindala et al., 2025). Disentangling these scenarios requires more detailed multi-wavelength spectral, timing, and polarimetry measurements, as well as the development of simulations and data-fitting models. If some of these alternative scenarios are at work, such as the scattering off the jet walls or disk winds, they may also contribute to the polarization signal in the hard state.

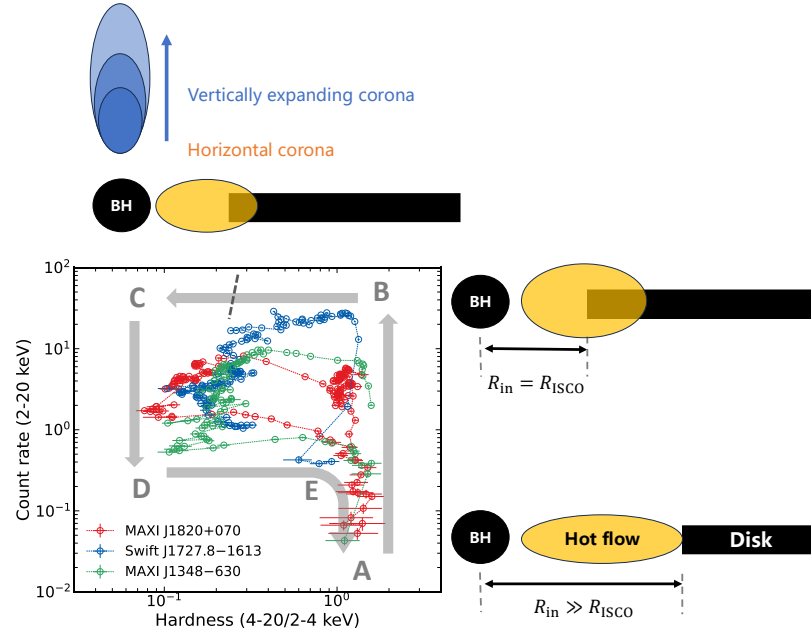


**Fig. 7** Sketch of hypothetical accretion geometries of BH XRBs along the hardness-intensity diagram.

### 4.3 Soft state (Region C to D)

The soft state is believed to be described by the standard optically thick, geometrically thin disk (Shakura and Sunyaev, 1973; Novikov and Thorne, 1973), with  $R_{\text{in}} = R_{\text{ISCO}}$  (Steiner et al., 2010) and low X-ray variability. Therefore, there are no X-ray reverberation results for the soft state. Compelling evidence supporting the standard disk scenario with  $R_{\text{in}} = R_{\text{ISCO}}$ , is the observed  $L_{\text{disk}} \propto T^4$  relation. This relation has been seen in the soft state for a number of sources where  $L_{\text{disk}}$  changes by nearly two orders of magnitude (Kubota et al., 2001; Kubota and Makishima, 2004; Gierliński and Done, 2004). This scaling indicates a constant inner disk radius, which is naturally identified with the ISCO.

Fitting relativistic disk thermal emission models to soft state X-ray spectra is one of the leading techniques to measure BH spin parameters (continuum fitting, Zhang et al., 1997; Gou et al., 2011; McClintock et al., 2014). This method typically assumes no emission within the ISCO radius (the plugging region). However, three-dimensional general relativistic magneto-hydrodynamic (GRMHD) simulations have shown that the plugging region could contribute with non-negligible emission to the total X-ray spectrum (e.g., Zhu et al., 2012; Mummery and Stone, 2024). In several cases, emission from this region is found to be essential for adequately modeling soft-state X-ray spectra (e.g., Fabian et al., 2020; Mummery et al., 2024b). This “extra” component may potentially affect continuum-fitting black hole spin measurements (e.g., Mummery et al., 2024a). The significance of plunging region emission increases for lower black hole spins, which is attributable to the greater extent of the emission region. (see Figure 11 of Mummery et al. 2024a). It has also been suggested that the plunging region may have its signature in X-ray polarization measurements (Chan et al., 2025).

Most IXPE observations in the soft state are well described by the standard disk model with  $R_{\text{in}} = R_{\text{ISCO}}$ . The variation of PD and PA with energy provides an independent method for measuring BH spins (Dovčiak et al., 2008; Mikusincova et al., 2023). Currently, spin constraints using polarimetric data have been obtained for four sources. The polarimetric data for 4U 1957+115, Cygnus X-1 and GRS 1739–278 suggest a significant role of returning radiation (Marra et al., 2024; Steiner et al., 2024; Zhao et al., 2026), which indicates a high BH spin ( $a_* > 0.96$  for 4U 1957+115 and Cygnus X-1,  $a_* > 0.991$  for GRS 1739–278). These constraints are consistent with previous spin measurements for these three sources using either continuum fitting (e.g.,  $a_* > 0.9$  for 4U 1957+115, Nowak et al. 2012;  $a_* > 0.9985$  for Cygnus X-1, Zhao et al. 2021) or reflection methods (e.g.,  $a_* = 0.95^{+0.02}_{-0.04}$  for 4U 1957+115, Draghis et al. 2023;  $0.93 < a_* < 0.96$  for Cygnus X-1, Walton et al. 2016;  $0.90 < a_* < 0.99$  for GRS 1739–278, Draghis et al. 2024). As for LMC X-3, only an upper limit is obtained for the BH spin from polarimetric data ( $a_* < 0.7$ , Svoboda et al. 2024b), which is also consistent with previous measurements using the continuum fitting method (e.g.,  $a_* = 0.25^{+0.20}_{-0.29}$ , Steiner et al. 2014).

However, there is an exceptional case, 4U 1630–47, where the high PD ( $\sim 8.6\%$ ) is incompatible with the standard accretion disk (Kushwaha et al., 2023; Ratheesh et al., 2024). Several potential explanations have been proposed to account for this high PD, including the returning radiation effect, an outflowing disk atmosphere (Nitindala

et al., 2025), and electron or ion anisotropies; however, none of these explanations fully explains the observations to date (Krawczynski et al., 2024).

A high-energy power-law tail, often extending from 10 keV to 1 MeV without a clear cutoff, is frequently observed in the soft state spectra of black hole X-ray binaries (Grove et al., 1998; McConnell et al., 2002). Such a tail has also been detected in the hard and intermediate states, superimposed on the thermal Comptonization component (e.g., Del Santo et al., 2008; Zdziarski et al., 2021). In the soft state, the tail is generally attributed to Compton scattering by a non-thermal electron population (i.e., the electron energy distribution is not a Maxwellian), likely accelerated by magnetic reconnection (Beloborodov, 2017; Ball et al., 2018; Sridhar et al., 2023) or shocks (Grošelj et al., 2024). However, the spatial location of these non-thermal electrons remains unknown; they could reside in active regions above the disk (Zdziarski and Gierliński, 2004) or in the plunging region (Hankla et al., 2022).

Although the power-law component is often weak in the soft state, it can still illuminate the disk and produce reflection features. It has been proposed that the reflection fraction (i.e., the ratio of reflected to direct coronal flux) is higher in the soft state than in the hard state (Zdziarski et al., 2003; Gilfanov and Merloni, 2014; Steiner et al., 2016). This suggests that the corona is more compact in the soft state, such that light-bending effects enhance the illumination of the disk (Miniutti and Fabian, 2004). Recently, evidence has emerged indicating that returning radiation may also play a role in shaping reflection features in the soft state (Connors et al., 2021; Mirzaev et al., 2024a). This effect does not appear to significantly affect black hole spin measurements (Das et al., 2025), but its implications for our understanding of coronal geometry remain to be explored using larger source samples and more proper modeling (Mirzaev et al., 2024b).

#### 4.4 Soft to hard transition (Region D to A)

The soft-to-hard state transition can occur at relatively low luminosities, e.g.,  $L_X/L_{\text{Edd}} < 1\%$  (Petrucci et al., 2014). Throughout this transition, the source evolves back through lower-luminosity variants of the soft intermediate and hard intermediate states, ultimately returning to the low-hard state. In the case of MAXI J1820+070, the transition was monitored by *Insight*-HXMT, which revealed that  $R_{\text{in}}$  gradually increased from 1 to 10  $R_{\text{ISCO}}$  (D to E, Fan et al. 2024a). However, this may not be a general behavior, as observations of other sources remain scarce and the data quality is often lower than that of the brighter hard-to-soft transitions. During this same transition, time lags between the X-ray, optical, and radio bands were detected and interpreted as evidence for a magnetically arrested disk (MAD) state, in which the radial magnetic force is sufficient to balance the gravitational force (You et al., 2023). These observed lags are thought to trace the process of magnetic field accumulation. In this scenario, the accumulation of magnetic flux near the black hole first gets strong enough to power the corona (producing X-ray emission), and subsequently becomes strong enough to launch the jet (producing the radio emission). The optical lag is attributed to a thermal-viscous instability triggered by heating of the outer disk by the X-ray flare.

A study of failed outbursts in GX 339–4 also found that the disk is more truncated during the rising phase (A to E) than the decaying phase (E to A), despite similar luminosities (Wang-Ji et al., 2018; Wang et al., 2020). Such a phenomenon suggests that even within the hard state, the inner disk radius is not solely determined by the accretion rate. The accretion history of the system may also play a role. It is also consistent the idea that the inner disk radius is evolving within the hard state. IXPE captured Swift J1727.8–1613 twice in the dim soft state (region D, Svoboda et al. 2024a) and once during the soft-to-hard transition (near region E, Podgorný et al. 2024). Compared to the bright hard and hard-intermediate states (PD  $\sim$  3–4%, Ingram et al. 2024), the PD drops to  $< 1\%$  in the dim soft state. At the end of the soft-to-hard transition, both the PD and PA return to the values observed in the bright hard state at similar hardness, despite the luminosity being over an order of magnitude lower (Podgorný et al., 2024). This suggests a similar coronal geometry in both the bright and dim hard states.

## 5 Concluding Remarks

Over the past decades, X-ray techniques have matured and become powerful tools for studying the accretion geometry of BH XRBs. Understanding this geometry is essential for controlling systematic uncertainties when using observational data to address fundamental questions, such as testing gravity theories (e.g., Liu et al., 2019; Bambi et al., 2021) or understanding black hole spin distributions (e.g., Draghis et al., 2024; Zdziarski et al., 2024). Based on a synthesis of spectral-timing results available in the literature, the following picture of the disk-corona system emerges:

1. The standard accretion disk is truncated at large radii in the *low hard* state, when the accretion rate is low ( $L_X/L_{\text{Edd}} < 1\%$ ). The radially extended hot inner flow may act as the corona, which is also consistent with X-ray polarimetric measurements.
2. In the *bright hard* state ( $L_X/L_{\text{Edd}} > 3\text{--}4\%$ ), the disk appears to extend close to the innermost stable circular orbit ( $R_{\text{ISCO}}$ ), before the state transition.
3. During the hard-to-soft transition, the disk remains near  $R_{\text{ISCO}}$ , while the corona expands vertically. X-ray polarimetry suggests that a horizontally extended coronal component may still be present (Ingram et al., 2024). A dual-corona configuration may be needed to simultaneously interpret the X-ray spectral, timing, and polarimetric data (see Figure 7). However, a self-consistent theoretical framework for this scenario is still lacking.

IXPE observations over the past few years have significantly advanced our understanding of BH accretion geometries. Some results align with the picture established by traditional spectral-timing studies, while others challenge the traditional view (e.g., Ratheesh et al., 2024; Ewing et al., 2025). The implications of these challenges remain uncertain, as high-sensitivity X-ray polarimetry is still a relatively young field. Nevertheless, several new accretion configurations — such as an outflowing corona (Poutanen et al., 2023), a scattering disk wind (Nitindala et al., 2025), and a warped disk (Krawczynski et al., 2022) — have already been proposed based on IXPE results. Meanwhile, some older models (e.g., lamppost and spherical coronal geometries) have

been ruled out (Krawczynski et al., 2022). An important next step is to determine which of these configurations most realistically explains the full suite of X-ray (and multi-wavelength) observations. The enhanced X-ray Timing and Polarimetry mission (eXTP), planned for launch in 2030 (Zhang et al., 2016, 2025; Bu et al., 2025), will further push the field forward. eXTP will carry three X-ray polarimeters with a total effective area five times larger than that of IXPE, as well as a separate spectrometer capable of providing simultaneous spectral and timing data. Such synergistic observations are crucial for breaking degeneracies and distinguishing between different scenarios (e.g., Ingram et al., 2024; Mastroserio et al., 2025).

The X-Ray Imaging and Spectroscopy Mission (XRISM; Tashiro et al. 2020), launched in September 2023, is also expected to provide new insights into BH XRBs, thanks to its high-energy-resolution microcalorimeter, *Resolve*. This high energy resolution makes it possible to distinguish subtle spectral features and place tighter constraints on model parameters (e.g., García et al., 2022b; Liu et al., 2025). Some initial results from XRISM have already shown its capability in separating the broad iron line and the narrow features (Draghis et al., 2025; Brenneman et al., 2025). Fitting of the broad iron line in Cygnus X-1 finds the inner disk inclination angle to be 30 degrees higher than the binary inclination angle, indicating a warped disk (Draghis et al., 2025). The New Advanced Telescope for High-ENergy Astrophysics (NewAthena; Cruise et al. 2025), a flagship mission planned for the late 2030s, will also carry a microcalorimeter spectrometer, but with a significantly larger effective area. NewAthena will enable more detailed studies of BH XRBs, as it can collect the same number of photons in just one-fourth of the exposure time required by XRISM (at 6 keV) if the gate valve shielding the Resolve instrument can be opened in the future, or one-seventh if the gate valve remains closed.

## 6 Statements and Declarations

**Acknowledgements:** HL thanks the anonymous referee for their insightful comments. HL also thanks Ningyue Fan, Mariano Mendez, and Federico Garcia for helpful discussions, and Cosimo Bambi for proofreading the manuscript. HL acknowledges support from the IAU-Gruber Foundation Fellowship.

**Funding information:** not applicable.

**Author contributions:** H.L. prepared this manuscript as a single author.

**Ethics declaration:** not applicable.

**Data availability:** No datasets were generated or analyzed.

## References

Abbott R, Abbott TD, Abraham S, et al (2021a) GWTC-2: Compact Binary Coalescences Observed by LIGO and Virgo during the First Half of the Third Observing Run. *Physical Review X* 11(2):021053. <https://doi.org/10.1103/PhysRevX.11.021053>, [arXiv:2010.14527](https://arxiv.org/abs/2010.14527) [gr-qc]

- Abbott R, Abbott TD, Abraham S, et al (2021b) Population Properties of Compact Objects from the Second LIGO-Virgo Gravitational-Wave Transient Catalog. *ApJ* 913(1):L7. <https://doi.org/10.3847/2041-8213/abe949>, [arXiv:2010.14533](https://arxiv.org/abs/2010.14533) [astro-ph.HE]
- Abbott R, Abbott TD, Acernese F, et al (2023) Population of Merging Compact Binaries Inferred Using Gravitational Waves through GWTC-3. *Physical Review X* 13(1):011048. <https://doi.org/10.1103/PhysRevX.13.011048>, [arXiv:2111.03634](https://arxiv.org/abs/2111.03634) [astro-ph.HE]
- Abdikamalov AB, Ayzenberg D, Bambi C, et al (2020) Testing the Kerr Black Hole Hypothesis Using X-Ray Reflection Spectroscopy and a Thin Disk Model with Finite Thickness. *ApJ* 899(1):80. <https://doi.org/10.3847/1538-4357/aba625>, [arXiv:2003.09663](https://arxiv.org/abs/2003.09663) [astro-ph.HE]
- Adegoke OK, García JA, Connors RMT, et al (2024) Characterizing the Broadband Reflection Spectrum of MAXI J1803-298 during Its 2021 Outburst with NuSTAR and NICER. *ApJ* 977(1):26. <https://doi.org/10.3847/1538-4357/ad82e9>, [arXiv:2410.01134](https://arxiv.org/abs/2410.01134) [astro-ph.HE]
- Alabarta K, Altamirano D, Méndez M, et al (2021) Failed-transition outbursts in black hole low-mass X-ray binaries. *MNRAS* 507(4):5507–5522. <https://doi.org/10.1093/mnras/stab2241>, [arXiv:2107.10035](https://arxiv.org/abs/2107.10035) [astro-ph.HE]
- Alabarta K, Méndez M, García F, et al (2025) Geometry of the Comptonization Region of MAXI J1348-630 through Type-C Quasiperiodic Oscillations with NICER. *ApJ* 980(2):251. <https://doi.org/10.3847/1538-4357/ada7f9>, [arXiv:2409.14883](https://arxiv.org/abs/2409.14883) [astro-ph.HE]
- Atri P, Miller-Jones JCA, Bahramian A, et al (2020) A radio parallax to the black hole X-ray binary MAXI J1820+070. *MNRAS* 493(1):L81–L86. <https://doi.org/10.1093/mnrasl/slaa010>, [arXiv:1912.04525](https://arxiv.org/abs/1912.04525) [astro-ph.HE]
- Avakyan A, Neumann M, Zainab A, et al (2023) XRBcats: Galactic low-mass X-ray binary catalogue. *A&A* 675:A199. <https://doi.org/10.1051/0004-6361/202346522>, [arXiv:2303.16168](https://arxiv.org/abs/2303.16168) [astro-ph.HE]
- Ball D, Sironi L, Özel F (2018) Electron and Proton Acceleration in Trans-relativistic Magnetic Reconnection: Dependence on Plasma Beta and Magnetization. *ApJ* 862(1):80. <https://doi.org/10.3847/1538-4357/aac820>, [arXiv:1803.05556](https://arxiv.org/abs/1803.05556) [astro-ph.HE]
- Ballantyne DR, Ross RR, Fabian AC (2001) X-ray reflection by photoionized accretion discs. *MNRAS* 327(1):10–22. <https://doi.org/10.1046/j.1365-8711.2001.04432.x>, [arXiv:astro-ph/0102040](https://arxiv.org/abs/astro-ph/0102040) [astro-ph]
- Bambi C (2017) Testing black hole candidates with electromagnetic radiation. *Reviews*

- of Modern Physics 89(2):025001. <https://doi.org/10.1103/RevModPhys.89.025001>, [arXiv:1509.03884](https://arxiv.org/abs/1509.03884) [gr-qc]
- Bambi C (2024a) A Tutorial on the Strong Gravity Effects in Black Hole X-Ray Spectra. *Universe* 10(12):451. <https://doi.org/10.3390/universe10120451>
- Bambi C (2024b) Testing General Relativity with Black Hole X-Ray Data. *Physics of Particles and Nuclei* 55(6):1420–1425. <https://doi.org/10.1134/S106377962470103X>, [arXiv:2312.05857](https://arxiv.org/abs/2312.05857) [gr-qc]
- Bambi C, Brenneman LW, Dauser T, et al (2021) Towards Precision Measurements of Accreting Black Holes Using X-Ray Reflection Spectroscopy. *Space Sci. Rev.* 217(5):65. <https://doi.org/10.1007/s11214-021-00841-8>, [arXiv:2011.04792](https://arxiv.org/abs/2011.04792) [astro-ph.HE]
- Bardeen JM, Petterson JA (1975) The Lense-Thirring Effect and Accretion Disks around Kerr Black Holes. *ApJ* 195:L65. <https://doi.org/10.1086/181711>
- Begelman MC, Armitage PJ (2014) A Mechanism for Hysteresis in Black Hole Binary State Transitions. *ApJ* 782(2):L18. <https://doi.org/10.1088/2041-8205/782/2/L18>, [arXiv:1401.5475](https://arxiv.org/abs/1401.5475) [astro-ph.HE]
- Bellavita C, García F, Méndez M, et al (2022) vKomph: a variable Comptonization model for low-frequency quasi-periodic oscillations in black hole X-ray binaries. *MNRAS* 515(2):2099–2109. <https://doi.org/10.1093/mnras/stac1922>, [arXiv:2206.13609](https://arxiv.org/abs/2206.13609) [astro-ph.HE]
- Belloni T, Klein-Wolt M, Méndez M, et al (2000) A model-independent analysis of the variability of GRS 1915+105. *A&A* 355:271–290. <https://doi.org/10.48550/arXiv.astro-ph/0001103>, [arXiv:astro-ph/0001103](https://arxiv.org/abs/astro-ph/0001103) [astro-ph]
- Belloni T, Homan J, Casella P, et al (2005) The evolution of the timing properties of the black-hole transient GX 339-4 during its 2002/2003 outburst. *A&A* 440(1):207–222. <https://doi.org/10.1051/0004-6361:20042457>, [arXiv:astro-ph/0504577](https://arxiv.org/abs/astro-ph/0504577) [astro-ph]
- Belloni TM (2010) States and Transitions in Black Hole Binaries. In: Belloni T (ed) *Lecture Notes in Physics*, Berlin Springer Verlag, vol 794. p 53, [https://doi.org/10.1007/978-3-540-76937-8\\_3](https://doi.org/10.1007/978-3-540-76937-8_3)
- Belloni TM, Motta SE (2016) Transient Black Hole Binaries. In: Bambi C (ed) *Astrophysics of Black Holes: From Fundamental Aspects to Latest Developments*, p 61, [https://doi.org/10.1007/978-3-662-52859-4\\_2](https://doi.org/10.1007/978-3-662-52859-4_2), [arXiv:1603.07872](https://arxiv.org/abs/1603.07872)
- Beloborodov AM (1999) Plasma Ejection from Magnetic Flares and the X-Ray Spectrum of Cygnus X-1. *ApJ* 510(2):L123–L126. <https://doi.org/10.1086/311810>, [arXiv:astro-ph/9809383](https://arxiv.org/abs/astro-ph/9809383) [astro-ph]

- Beloborodov AM (2017) Radiative Magnetic Reconnection Near Accreting Black Holes. *ApJ* 850(2):141. <https://doi.org/10.3847/1538-4357/aa8f4f>, [arXiv:1701.02847](https://arxiv.org/abs/1701.02847) [astro-ph.HE]
- Bolton CT (1972) Identification of Cygnus X-1 with HDE 226868. *Nature* 235(5336):271–273. <https://doi.org/10.1038/235271b0>
- Bouchet T, Rodriguez J, Cangemi F, et al (2024) INTEGRAL/IBIS polarization detection in the hard and soft intermediate states of Swift J1727.8–1613. *A&A* 688:L5. <https://doi.org/10.1051/0004-6361/202450826>, [arXiv:2407.05871](https://arxiv.org/abs/2407.05871) [astro-ph.HE]
- Bowyer S, Byram ET, Chubb TA, et al (1965) Cosmic X-ray Sources. *Science* 147(3656):394–398. <https://doi.org/10.1126/science.147.3656.394>
- Brenneman LW, Reynolds CS (2006) Constraining Black Hole Spin via X-Ray Spectroscopy. *ApJ* 652(2):1028–1043. <https://doi.org/10.1086/508146>, [arXiv:astro-ph/0608502](https://arxiv.org/abs/astro-ph/0608502) [astro-ph]
- Brenneman LW, Madejski G, Fuerst F, et al (2014) Measuring the Coronal Properties of IC 4329A with NuSTAR. *ApJ* 781(2):83. <https://doi.org/10.1088/0004-637X/781/2/83>, [arXiv:1312.3563](https://arxiv.org/abs/1312.3563) [astro-ph.HE]
- Brenneman LW, Wilkins DR, Ogorzałek A, et al (2025) A Sharper View of the X-Ray Spectrum of MCG-6-30-15 with XRISM, XMM-Newton, and NuSTAR. *ApJ* 995(2):200. <https://doi.org/10.3847/1538-4357/ae1225>, [arXiv:2510.08926](https://arxiv.org/abs/2510.08926) [astro-ph.HE]
- Bright JS, Fender RP, Motta SE, et al (2020) An extremely powerful long-lived superluminal ejection from the black hole MAXI J1820+070. *Nature Astronomy* 4:697–703. <https://doi.org/10.1038/s41550-020-1023-5>, [arXiv:2003.01083](https://arxiv.org/abs/2003.01083) [astro-ph.HE]
- Bu Q, Zhang S (2023) Black holes: accretion processes in X-ray binaries. *arXiv e-prints* [arXiv:2310.20637](https://arxiv.org/abs/2310.20637). <https://doi.org/10.48550/arXiv.2310.20637>, [arXiv:2310.20637](https://arxiv.org/abs/2310.20637) [astro-ph.HE]
- Bu Q, Bambi C, Gou L, et al (2025) Probing the strong gravity region of black holes with eXTP. *Science China Physics, Mechanics, and Astronomy* 68(11):119504. <https://doi.org/10.1007/s11433-025-2789-2>, [arXiv:2506.08105](https://arxiv.org/abs/2506.08105) [astro-ph.HE]
- Buisson DJK, Fabian AC, Barret D, et al (2019) MAXI J1820+070 with NuSTAR I. An increase in variability frequency but a stable reflection spectrum: coronal properties and implications for the inner disc in black hole binaries. *MNRAS* 490(1):1350–1362. <https://doi.org/10.1093/mnras/stz2681>, [arXiv:1909.04688](https://arxiv.org/abs/1909.04688) [astro-ph.HE]
- Cadolle Bel M, Ribó M, Rodriguez J, et al (2007) Simultaneous Multiwavelength Observations of the Low/Hard State of the X-Ray Transient Source SWIFT

- J1753.5-0127. *ApJ* 659(1):549–560. <https://doi.org/10.1086/512004>, [arXiv:astro-ph/0612575](#) [astro-ph]
- Cao Z, Lucchini M, Markoff S, et al (2022) Evidence for an expanding corona based on spectral-timing modelling of multiple black hole X-ray binaries. *MNRAS* 509(2):2517–2531. <https://doi.org/10.1093/mnras/stab3080>, [arXiv:2110.10547](#) [astro-ph.HE]
- Casares J, Yanes-Rizo IV, Torres MAP, et al (2023) The orbital period, black hole mass, and distance to the X-ray transient GRS 1716-249 (=N Oph 93). *MNRAS* 526(4):5209–5219. <https://doi.org/10.1093/mnras/stad3068>, [arXiv:2310.11561](#) [astro-ph.HE]
- Chakrabarti SK, Debnath D, Nandi A, et al (2008) Evolution of the quasi-periodic oscillation frequency in GRO J1655-40 - Implications for accretion disk dynamics. *A&A* 489(3):L41–L44. <https://doi.org/10.1051/0004-6361:200810136>, [arXiv:0809.0876](#) [astro-ph]
- Chan HS, Begelman MC, Dexter J (2025) Polarimetric Signatures of Bulk Comptonization from within the Plunging Region of Accreting Black Holes. *arXiv e-prints* [arXiv:2504.15486](#). <https://doi.org/10.48550/arXiv.2504.15486>, [arXiv:2504.15486](#) [astro-ph.HE]
- Chandrasekhar S (1960) Radiative transfer
- Chauhan J, Miller-Jones JCA, Anderson GE, et al (2019) An H I absorption distance to the black hole candidate X-ray binary MAXI J1535-571. *MNRAS* 488(1):L129–L133. <https://doi.org/10.1093/mnrasl/slz113>, [arXiv:1905.08497](#) [astro-ph.HE]
- Chiang CY, Reis RC, Walton DJ, et al (2012) Re-examining the XMM-Newton spectrum of the black hole candidate XTE J1652-453. *MNRAS* 425(4):2436–2442. <https://doi.org/10.1111/j.1365-2966.2012.21591.x>, [arXiv:1207.0682](#) [astro-ph.HE]
- Connors RMT, García JA, Tomsick J, et al (2021) Reflection Modeling of the Black Hole Binary 4U 1630-47: The Disk Density and Returning Radiation. *ApJ* 909(2):146. <https://doi.org/10.3847/1538-4357/abdd2c>, [arXiv:2101.06343](#) [astro-ph.HE]
- Connors RMT, Tomsick JA, Draghis P, et al (2024) The High Energy X-ray Probe (HEX-P): probing accretion onto stellar mass black holes. *Frontiers in Astronomy and Space Sciences* 10:1292682. <https://doi.org/10.3389/fspas.2023.1292682>, [arXiv:2311.04782](#) [astro-ph.HE]
- Corbel S, Nowak MA, Fender RP, et al (2003) Radio/X-ray correlation in the low/hard state of GX 339-4. *A&A* 400:1007–1012. <https://doi.org/10.1051/0004-6361:20030090>, [arXiv:astro-ph/0301436](#) [astro-ph]

- Corbel S, Tomsick JA, Kaaret P (2006) On the Origin of Black Hole X-Ray Emission in Quiescence: Chandra Observations of XTE J1550-564 and H1743-322. *ApJ* 636(2):971–978. <https://doi.org/10.1086/498230>, [arXiv:astro-ph/0509870](https://arxiv.org/abs/astro-ph/0509870) [astro-ph]
- Coriat M, Fender RP, Dubus G (2012) Revisiting a fundamental test of the disc instability model for X-ray binaries. *MNRAS* 424(3):1991–2001. <https://doi.org/10.1111/j.1365-2966.2012.21339.x>, [arXiv:1205.5038](https://arxiv.org/abs/1205.5038) [astro-ph.HE]
- Corral-Santana JM, Casares J, Muñoz-Darias T, et al (2016) BlackCAT: A catalogue of stellar-mass black holes in X-ray transients. *A&A* 587:A61. <https://doi.org/10.1051/0004-6361/201527130>, [arXiv:1510.08869](https://arxiv.org/abs/1510.08869) [astro-ph.HE]
- Cruise M, Guainazzi M, Aird J, et al (2025) The NewAthena mission concept in the context of the next decade of X-ray astronomy. *Nature Astronomy* 9:36–44. <https://doi.org/10.1038/s41550-024-02416-3>, [arXiv:2501.03100](https://arxiv.org/abs/2501.03100) [astro-ph.IM]
- Dai X, Kochanek CS, Chartas G, et al (2010) The Sizes of the X-ray and Optical Emission Regions of RXJ 1131-1231. *ApJ* 709(1):278–285. <https://doi.org/10.1088/0004-637X/709/1/278>, [arXiv:0906.4342](https://arxiv.org/abs/0906.4342) [astro-ph.HE]
- Das D, Liu H, Zhang Z, et al (2025) Spin Constraints on 4U 1630-47 via combined Continuum Fitting and Reflection methods: a comparative study using Frequentist and Bayesian statistics. *arXiv e-prints* [arXiv:2509.09481](https://arxiv.org/abs/2509.09481). <https://doi.org/10.48550/arXiv.2509.09481>, [arXiv:2509.09481](https://arxiv.org/abs/2509.09481) [astro-ph.HE]
- Dauser T, Wilms J, Reynolds CS, et al (2010) Broad emission lines for a negatively spinning black hole. *MNRAS* 409(4):1534–1540. <https://doi.org/10.1111/j.1365-2966.2010.17393.x>, [arXiv:1007.4937](https://arxiv.org/abs/1007.4937) [astro-ph.HE]
- Dauser T, Garcia J, Wilms J, et al (2013) Irradiation of an accretion disc by a jet: general properties and implications for spin measurements of black holes. *MNRAS* 430(3):1694–1708. <https://doi.org/10.1093/mnras/sts710>, [arXiv:1301.4922](https://arxiv.org/abs/1301.4922) [astro-ph.HE]
- Davidson EM, Chauhan J, Lohfink A, et al (2025) Establishing a Connection between the Jet and the Corona in Black Hole Low-mass X-Ray Binaries. *ApJ* 994(1):54. <https://doi.org/10.3847/1538-4357/ae0a4d>, [arXiv:2505.07962](https://arxiv.org/abs/2505.07962) [astro-ph.HE]
- Davis SW, Blaes OM, Hubeny I, et al (2005) Relativistic Accretion Disk Models of High-State Black Hole X-Ray Binary Spectra. *ApJ* 621(1):372–387. <https://doi.org/10.1086/427278>, [arXiv:astro-ph/0408590](https://arxiv.org/abs/astro-ph/0408590) [astro-ph]
- De Rosa A, Uttley P, Gou L, et al (2019) Accretion in strong field gravity with eXTP. *Science China Physics, Mechanics, and Astronomy* 62(2):29504. <https://doi.org/10.1007/s11433-018-9297-0>, [arXiv:1812.04022](https://arxiv.org/abs/1812.04022) [astro-ph.HE]
- Del Santo M, Malzac J, Jourdain E, et al (2008) Spectral variability of GX339-4 in

- a hard-to-soft state transition. *MNRAS* 390(1):227–234. <https://doi.org/10.1111/j.1365-2966.2008.13672.x>, [arXiv:0807.1018](https://arxiv.org/abs/0807.1018) [astro-ph]
- DeMarco B, Zdziarski AA, Ponti G, et al (2021) The inner flow geometry in MAXI J1820+070 during hard and hard-intermediate states. *A&A* 654:A14. <https://doi.org/10.1051/0004-6361/202140567>, [arXiv:2102.07811](https://arxiv.org/abs/2102.07811) [astro-ph.HE]
- Dexter J, Begelman MC (2024) A relativistic outflow model of the X-ray polarization in Cyg X-1. *MNRAS* 528(1):L157–L160. <https://doi.org/10.1093/mnrasl/slada182>, [arXiv:2308.01963](https://arxiv.org/abs/2308.01963) [astro-ph.HE]
- Done C, Gierliński M, Kubota A (2007) Modelling the behaviour of accretion flows in X-ray binaries. Everything you always wanted to know about accretion but were afraid to ask. *A&A Rev.* 15(1):1–66. <https://doi.org/10.1007/s00159-007-0006-1>, [arXiv:0708.0148](https://arxiv.org/abs/0708.0148) [astro-ph]
- Dovčiak M, Karas V, Yaqoob T (2004) An Extended Scheme for Fitting X-Ray Data with Accretion Disk Spectra in the Strong Gravity Regime. *ApJS* 153(1):205–221. <https://doi.org/10.1086/421115>, [arXiv:astro-ph/0403541](https://arxiv.org/abs/astro-ph/0403541) [astro-ph]
- Dovčiak M, Muleri F, Goosmann RW, et al (2008) Thermal disc emission from a rotating black hole: X-ray polarization signatures. *MNRAS* 391(1):32–38. <https://doi.org/10.1111/j.1365-2966.2008.13872.x>, [arXiv:0809.0418](https://arxiv.org/abs/0809.0418) [astro-ph]
- Dovčiak M, Muleri F, Goosmann RW, et al (2011) Light-bending Scenario for Accreting Black Holes in X-ray Polarimetry. *ApJ* 731(1):75. <https://doi.org/10.1088/0004-637X/731/1/75>, [arXiv:1102.4247](https://arxiv.org/abs/1102.4247) [astro-ph.HE]
- Dovčiak M, Podgorný J, Svoboda J, et al (2024) IXPE View of BH XRBs during the First 2.5 Years of the Mission. *Galaxies* 12(5):54. <https://doi.org/10.3390/galaxies12050054>
- Draghis PA, Miller JM, Cackett EM, et al (2020) A New Spin on an Old Black Hole: NuSTAR Spectroscopy of EXO 1846-031. *ApJ* 900(1):78. <https://doi.org/10.3847/1538-4357/aba2ec>, [arXiv:2007.04324](https://arxiv.org/abs/2007.04324) [astro-ph.HE]
- Draghis PA, Miller JM, Zoghbi A, et al (2023) A Systematic View of Ten New Black Hole Spins. *ApJ* 946(1):19. <https://doi.org/10.3847/1538-4357/acafe7>, [arXiv:2210.02479](https://arxiv.org/abs/2210.02479) [astro-ph.HE]
- Draghis PA, Miller JM, Costantini E, et al (2024) Systematically Revisiting All NuSTAR Spins of Black Holes in X-Ray Binaries. *ApJ* 969(1):40. <https://doi.org/10.3847/1538-4357/ad43ea>, [arXiv:2311.16225](https://arxiv.org/abs/2311.16225) [astro-ph.HE]
- Draghis PA, Miller JM, Kara E, et al (2025) A XRISM View of Relativistic Reflection in Cygnus X-1. *ApJ* 995(1):L12. <https://doi.org/10.3847/2041-8213/ae2276>, [arXiv:2511.17338](https://arxiv.org/abs/2511.17338) [astro-ph.HE]

- Dumont AM, Collin S, Paletou F, et al (2003) Escape probability methods versus “exact” transfer for modelling the X-ray spectrum of Active Galactic Nuclei and X-ray binaries. *A&A* 407:13–30. <https://doi.org/10.1051/0004-6361:20030890>, [arXiv:astro-ph/0306297](https://arxiv.org/abs/astro-ph/0306297) [astro-ph]
- Ebisawa K, Życki P, Kubota A, et al (2003) Accretion Disk Spectra of Ultraluminous X-Ray Sources in Nearby Spiral Galaxies and Galactic Superluminal Jet Sources. *ApJ* 597(2):780–797. <https://doi.org/10.1086/378586>, [arXiv:astro-ph/0307392](https://arxiv.org/abs/astro-ph/0307392) [astro-ph]
- Emmanoulopoulos D, Papadakis IE, Dovčiak M, et al (2014) General relativistic modelling of the negative reverberation X-ray time delays in AGN. *MNRAS* 439(4):3931–3950. <https://doi.org/10.1093/mnras/stu249>, [arXiv:1402.0899](https://arxiv.org/abs/1402.0899) [astro-ph.HE]
- Esin AA, McClintock JE, Narayan R (1997) Advection-Dominated Accretion and the Spectral States of Black Hole X-Ray Binaries: Application to Nova Muscae 1991. *ApJ* 489(2):865–889. <https://doi.org/10.1086/304829>, [arXiv:astro-ph/9705237](https://arxiv.org/abs/astro-ph/9705237) [astro-ph]
- Ewing M, Parra M, Mastroserio G, et al (2025) The very high X-ray polarization of accreting black hole IGR J17091-3624 in the hard state. *MNRAS* 541(2):1774–1781. <https://doi.org/10.1093/mnras/staf859>, [arXiv:2503.22665](https://arxiv.org/abs/2503.22665) [astro-ph.HE]
- Fabian AC, Rees MJ, Stella L, et al (1989) X-ray fluorescence from the inner disc in Cygnus X-1. *MNRAS* 238:729–736. <https://doi.org/10.1093/mnras/238.3.729>
- Fabian AC, Iwasawa K, Reynolds CS, et al (2000) Broad Iron Lines in Active Galactic Nuclei. *PASP* 112(775):1145–1161. <https://doi.org/10.1086/316610>, [arXiv:astro-ph/0004366](https://arxiv.org/abs/astro-ph/0004366) [astro-ph]
- Fabian AC, Zoghbi A, Ross RR, et al (2009) Broad line emission from iron K- and L-shell transitions in the active galaxy 1H0707-495. *Nature* 459(7246):540–542. <https://doi.org/10.1038/nature08007>
- Fabian AC, Buisson DJ, Kosec P, et al (2020) The soft state of the black hole transient source MAXI J1820+070: emission from the edge of the plunge region? *MNRAS* 493(4):5389–5396. <https://doi.org/10.1093/mnras/staa564>, [arXiv:2002.09691](https://arxiv.org/abs/2002.09691) [astro-ph.HE]
- Fan N, Li S, Zhan R, et al (2024a) The 2018 Outburst of MAXI J1820+070 as Seen by Insight-HXMT. *ApJ* 969(1):61. <https://doi.org/10.3847/1538-4357/ad49a1>, [arXiv:2404.12161](https://arxiv.org/abs/2404.12161) [astro-ph.HE]
- Fan N, Steiner JF, Bambi C, et al (2024b) NICER Spectral and Timing Analysis of 4U 1630–47 and its Heartbeat State. *arXiv e-prints* [arXiv:2412.07621](https://arxiv.org/abs/2412.07621). <https://doi.org/10.48550/arXiv.2412.07621>, [arXiv:2412.07621](https://arxiv.org/abs/2412.07621) [astro-ph.HE]

- Fender RP, Belloni TM, Gallo E (2004) Towards a unified model for black hole X-ray binary jets. *MNRAS* 355(4):1105–1118. <https://doi.org/10.1111/j.1365-2966.2004.08384.x>, [arXiv:astro-ph/0409360](https://arxiv.org/abs/astro-ph/0409360) [astro-ph]
- Fender RP, Homan J, Belloni TM (2009) Jets from black hole X-ray binaries: testing, refining and extending empirical models for the coupling to X-rays. *MNRAS* 396(3):1370–1382. <https://doi.org/10.1111/j.1365-2966.2009.14841.x>, [arXiv:0903.5166](https://arxiv.org/abs/0903.5166) [astro-ph.HE]
- Fishbach M, Kalogera V (2022) Apples and Oranges: Comparing Black Holes in X-Ray Binaries and Gravitational-wave Sources. *ApJ* 929(2):L26. <https://doi.org/10.3847/2041-8213/ac64a5>, [arXiv:2111.02935](https://arxiv.org/abs/2111.02935) [astro-ph.HE]
- Fürst F, Nowak MA, Tomsick JA, et al (2015) The Complex Accretion Geometry of GX 339-4 as Seen by NuSTAR and Swift. *ApJ* 808(2):122. <https://doi.org/10.1088/0004-637X/808/2/122>, [arXiv:1506.01381](https://arxiv.org/abs/1506.01381) [astro-ph.HE]
- Furst F, Tomsick JA, Yamaoka K, et al (2016) GRS 1739-278 Observed at Very Low Luminosity with XMM-Newton and NuSTAR. *ApJ* 832(2):115. <https://doi.org/10.3847/0004-637X/832/2/115>, [arXiv:1609.07530](https://arxiv.org/abs/1609.07530) [astro-ph.HE]
- García F, Méndez M, Karpouzas K, et al (2021) A two-component Comptonization model for the type-B QPO in MAXI J1348-630. *MNRAS* 501(3):3173–3182. <https://doi.org/10.1093/mnras/staa3944>, [arXiv:2012.10354](https://arxiv.org/abs/2012.10354) [astro-ph.HE]
- García F, Karpouzas K, Méndez M, et al (2022a) The evolving properties of the corona of GRS 1915+105: a spectral-timing perspective through variable-Comptonization modelling. *MNRAS* 513(3):4196–4207. <https://doi.org/10.1093/mnras/stac1202>, [arXiv:2204.13279](https://arxiv.org/abs/2204.13279) [astro-ph.HE]
- García J, Kallman TR (2010) X-ray Reflected Spectra from Accretion Disk Models. I. Constant Density Atmospheres. *ApJ* 718(2):695–706. <https://doi.org/10.1088/0004-637X/718/2/695>, [arXiv:1006.0485](https://arxiv.org/abs/1006.0485) [astro-ph.HE]
- García JA, Steiner JF, McClintock JE, et al (2015) X-Ray Reflection Spectroscopy of the Black Hole GX 339–4: Exploring the Hard State with Unprecedented Sensitivity. *ApJ* 813(2):84. <https://doi.org/10.1088/0004-637X/813/2/84>, [arXiv:1505.03607](https://arxiv.org/abs/1505.03607) [astro-ph.HE]
- García JA, Tomsick JA, Sridhar N, et al (2019) The 2017 Failed Outburst of GX 339-4: Relativistic X-Ray Reflection near the Black Hole Revealed by NuSTAR and Swift Spectroscopy. *ApJ* 885(1):48. <https://doi.org/10.3847/1538-4357/ab384f>, [arXiv:1908.00965](https://arxiv.org/abs/1908.00965) [astro-ph.HE]
- García JA, Dauser T, Ludlam R, et al (2022b) Relativistic X-Ray Reflection Models for Accreting Neutron Stars. *ApJ* 926(1):13. <https://doi.org/10.3847/1538-4357/ac3cb7>, [arXiv:2111.12838](https://arxiv.org/abs/2111.12838) [astro-ph.HE]

- Gates DEA, Truong C, Sahu A, et al (2024) On the Morphology of Relativistically Broadened Line Emission from Axisymmetric Equatorial Accretion Disks. arXiv e-prints arXiv:2411.14338. <https://doi.org/10.48550/arXiv.2411.14338>, [arXiv:2411.14338](https://arxiv.org/abs/2411.14338) [astro-ph.HE]
- George IM, Fabian AC (1991) X-ray reflection from cold matter in Active Galactic Nuclei and X-ray binaries. MNRAS 249:352. <https://doi.org/10.1093/mnras/249.2.352>
- Gierliński M, Done C (2003) The X-ray/ $\gamma$ -ray spectrum of XTE J1550-564 in the very high state. MNRAS 342(4):1083–1092. <https://doi.org/10.1046/j.1365-8711.2003.06591.x>, [arXiv:astro-ph/0212384](https://arxiv.org/abs/astro-ph/0212384) [astro-ph]
- Gierliński M, Done C (2004) Black hole accretion discs: reality confronts theory. MNRAS 347(3):885–894. <https://doi.org/10.1111/j.1365-2966.2004.07266.x>, [arXiv:astro-ph/0307333](https://arxiv.org/abs/astro-ph/0307333) [astro-ph]
- Gilfanov M, Merloni A (2014) Observational Appearance of Black Holes in X-Ray Binaries and AGN. Space Sci. Rev. 183(1-4):121–148. <https://doi.org/10.1007/s11214-014-0071-5>
- Goosmann RW, Gaskell CM (2007) Modeling optical and UV polarization of AGNs. I. Imprints of individual scattering regions. A&A 465(1):129–145. <https://doi.org/10.1051/0004-6361:20053555>, [arXiv:astro-ph/0507072](https://arxiv.org/abs/astro-ph/0507072) [astro-ph]
- Gou L, McClintock JE, Reid MJ, et al (2011) The Extreme Spin of the Black Hole in Cygnus X-1. ApJ 742(2):85. <https://doi.org/10.1088/0004-637X/742/2/85>, [arXiv:1106.3690](https://arxiv.org/abs/1106.3690) [astro-ph.HE]
- Greiner J, Dennerl K, Predehl P (1996) ROSAT observation of GRS 1739-278. A&A 314:L21–L24. [arXiv:astro-ph/9608184](https://arxiv.org/abs/astro-ph/9608184) [astro-ph]
- Grove JE, Johnson WN, Kroeger RA, et al (1998) Gamma-Ray Spectral States of Galactic Black Hole Candidates. ApJ 500(2):899–908. <https://doi.org/10.1086/305746>, [arXiv:astro-ph/9802242](https://arxiv.org/abs/astro-ph/9802242) [astro-ph]
- Grošelj D, Hakobyan H, Beloborodov AM, et al (2024) Radiative Particle-in-Cell Simulations of Turbulent Comptonization in Magnetized Black-Hole Coronae. Phys. Rev. Lett. 132(8):085202. <https://doi.org/10.1103/PhysRevLett.132.085202>, [arXiv:2301.11327](https://arxiv.org/abs/2301.11327) [astro-ph.HE]
- Haardt F, Maraschi L (1991) A Two-Phase Model for the X-Ray Emission from Seyfert Galaxies. ApJ 380:L51. <https://doi.org/10.1086/186171>
- Haardt F, Maraschi L (1993) X-Ray Spectra from Two-Phase Accretion Disks. ApJ 413:507. <https://doi.org/10.1086/173020>

- Haardt F, Maraschi L, Ghisellini G (1994) A Model for the X-Ray and Ultraviolet Emission from Seyfert Galaxies and Galactic Black Holes. *ApJ* 432:L95. <https://doi.org/10.1086/187520>, [arXiv:astro-ph/9405059](https://arxiv.org/abs/astro-ph/9405059) [astro-ph]
- Hankla AM, Scepi N, Dexter J (2022) Non-thermal emission from the plunging region: a model for the high-energy tail of black hole X-ray binary soft states. *MNRAS* 515(1):775–784. <https://doi.org/10.1093/mnras/stac1785>, [arXiv:2206.12018](https://arxiv.org/abs/2206.12018) [astro-ph.HE]
- Heil LM, Uttley P, Klein-Wolt M (2015) Power colours: simple X-ray binary variability comparison. *MNRAS* 448(4):3339–3347. <https://doi.org/10.1093/mnras/stv191>, [arXiv:1405.2024](https://arxiv.org/abs/1405.2024) [astro-ph.HE]
- Hirsch M, Pottschmidt K, Smith DM, et al (2020) X-ray spectral and flux variability of the microquasar GRS 1758-258 on timescales from weeks to years. *A&A* 636:A51. <https://doi.org/10.1051/0004-6361/201834647>, [arXiv:1912.09958](https://arxiv.org/abs/1912.09958) [astro-ph.HE]
- Homan J, Belloni T (2005) The Evolution of Black Hole States. *Ap&SS* 300(1-3):107–117. <https://doi.org/10.1007/s10509-005-1197-4>, [arXiv:astro-ph/0412597](https://arxiv.org/abs/astro-ph/0412597) [astro-ph]
- Homan J, Bright J, Motta SE, et al (2020) A Rapid Change in X-Ray Variability and a Jet Ejection in the Black Hole Transient MAXI J1820+070. *ApJ* 891(2):L29. <https://doi.org/10.3847/2041-8213/ab7932>, [arXiv:2003.01012](https://arxiv.org/abs/2003.01012) [astro-ph.HE]
- Ichimaru S (1977) Bimodal behavior of accretion disks: theory and application to Cygnus X-1 transitions. *ApJ* 214:840–855. <https://doi.org/10.1086/155314>
- Ingram A, Done C (2011) A physical model for the continuum variability and quasi-periodic oscillation in accreting black holes. *MNRAS* 415(3):2323–2335. <https://doi.org/10.1111/j.1365-2966.2011.18860.x>, [arXiv:1101.2336](https://arxiv.org/abs/1101.2336) [astro-ph.SR]
- Ingram A, Done C (2012) Modelling variability in black hole binaries: linking simulations to observations. *MNRAS* 419(3):2369–2378. <https://doi.org/10.1111/j.1365-2966.2011.19885.x>, [arXiv:1108.0789](https://arxiv.org/abs/1108.0789) [astro-ph.HE]
- Ingram A, Done C, Fragile PC (2009) Low-frequency quasi-periodic oscillations spectra and Lense-Thirring precession. *MNRAS* 397(1):L101–L105. <https://doi.org/10.1111/j.1745-3933.2009.00693.x>, [arXiv:0901.1238](https://arxiv.org/abs/0901.1238) [astro-ph.SR]
- Ingram A, Mastroserio G, Dauser T, et al (2019) A public relativistic transfer function model for X-ray reverberation mapping of accreting black holes. *MNRAS* 488(1):324–347. <https://doi.org/10.1093/mnras/stz1720>, [arXiv:1906.08310](https://arxiv.org/abs/1906.08310) [astro-ph.HE]
- Ingram A, Bollemeijer N, Veledina A, et al (2024) Tracking the X-Ray Polarization of the Black Hole Transient Swift J1727.8–1613 during a State Transition. *ApJ* 968(2):76. <https://doi.org/10.3847/1538-4357/ad3faf>, [arXiv:2311.05497](https://arxiv.org/abs/2311.05497)

[astro-ph.HE]

- Ingram AR, Motta SE (2019) A review of quasi-periodic oscillations from black hole X-ray binaries: Observation and theory. *New A Rev.* 85:101524. <https://doi.org/10.1016/j.newar.2020.101524>, [arXiv:2001.08758](https://arxiv.org/abs/2001.08758) [astro-ph.HE]
- Iyer N, Nandi A, Mandal S (2015) Determination of the Mass of IGR J17091-3624 from “Spectro-temporal” Variations during the Onset Phase of the 2011 Outburst. *ApJ* 807(1):108. <https://doi.org/10.1088/0004-637X/807/1/108>, [arXiv:1505.02529](https://arxiv.org/abs/1505.02529) [astro-ph.HE]
- Jia N, Zhao X, Gou L, et al (2022) Detailed analysis on the reflection component for the black hole candidate MAXI J1348-630. *MNRAS* 511(3):3125–3132. <https://doi.org/10.1093/mnras/stac121>, [arXiv:2201.01207](https://arxiv.org/abs/2201.01207) [astro-ph.HE]
- Jiang J (2024) Fifty Years After the Discovery of the First Stellar-Mass Black Hole: A Review of Cyg X-1. *Galaxies* 12(6):80. <https://doi.org/10.3390/galaxies12060080>, [arXiv:2411.12507](https://arxiv.org/abs/2411.12507) [astro-ph.HE]
- Jiang J, Fabian AC, Wang J, et al (2019) High-density reflection spectroscopy: I. A case study of GX 339-4. *MNRAS* 484(2):1972–1982. <https://doi.org/10.1093/mnras/stz095>, [arXiv:1901.01739](https://arxiv.org/abs/1901.01739) [astro-ph.HE]
- Jiang J, Fürst F, Walton DJ, et al (2020) A NuSTAR view of GRS 1716-249 in the hard and intermediate states. *MNRAS* 492(2):1947–1956. <https://doi.org/10.1093/mnras/staa017>, [arXiv:1912.13215](https://arxiv.org/abs/1912.13215) [astro-ph.HE]
- Jiang J, Abdikamalov AB, Bambi C, et al (2022) Black hole spin measurements based on a thin disc model with finite thickness - I. An example study of MCG-06-30-15. *MNRAS* 514(3):3246–3259. <https://doi.org/10.1093/mnras/stac1369>, [arXiv:2205.06696](https://arxiv.org/abs/2205.06696) [astro-ph.HE]
- Kara E, García J (2025) Supermassive Black Holes in X-Rays: From Standard Accretion to Extreme Transients. *ARA&A* 63(1):379–430. <https://doi.org/10.1146/annurev-astro-071221-052844>, [arXiv:2503.22791](https://arxiv.org/abs/2503.22791) [astro-ph.HE]
- Kara E, Zoghbi A, Marinucci A, et al (2015) Iron K and Compton hump reverberation in SWIFT J2127.4+5654 and NGC 1365 revealed by NuSTAR and XMM-Newton. *MNRAS* 446(1):737–749. <https://doi.org/10.1093/mnras/stu2136>, [arXiv:1410.3357](https://arxiv.org/abs/1410.3357) [astro-ph.HE]
- Kara E, Alston WN, Fabian AC, et al (2016) A global look at X-ray time lags in Seyfert galaxies. *MNRAS* 462(1):511–531. <https://doi.org/10.1093/mnras/stw1695>, [arXiv:1605.02631](https://arxiv.org/abs/1605.02631) [astro-ph.HE]
- Kara E, Steiner JF, Fabian AC, et al (2019) The corona contracts in a black-hole transient. *Nature* 565(7738):198–201. <https://doi.org/10.1038/s41586-018-0803-x>,

[arXiv:1901.03877](https://arxiv.org/abs/1901.03877) [astro-ph.HE]

- Kawamura T, Done C, Takahashi T (2023) The origin of long soft lags and the nature of the hard-intermediate state in black hole binaries. *MNRAS* 525(1):1280–1287. <https://doi.org/10.1093/mnras/stad2338>, [arXiv:2304.12003](https://arxiv.org/abs/2304.12003) [astro-ph.HE]
- King AL, Walton DJ, Miller JM, et al (2014) The Disk Wind in the Rapidly Spinning Stellar-mass Black Hole 4U 1630-472 Observed with NuSTAR. *ApJ* 784(1):L2. <https://doi.org/10.1088/2041-8205/784/1/L2>, [arXiv:1401.3646](https://arxiv.org/abs/1401.3646) [astro-ph.HE]
- Koljonen KII, Russell DM, Corral-Santana JM, et al (2016) A ‘high-hard’ outburst of the black hole X-ray binary GS 1354-64. *MNRAS* 460(1):942–955. <https://doi.org/10.1093/mnras/stw1007>, [arXiv:1602.06414](https://arxiv.org/abs/1602.06414) [astro-ph.HE]
- Kong AKH, McClintock JE, Garcia MR, et al (2002) The X-Ray Spectra of Black Hole X-Ray Novae in Quiescence as Measured by Chandra. *ApJ* 570(1):277–286. <https://doi.org/10.1086/339501>, [arXiv:astro-ph/0111134](https://arxiv.org/abs/astro-ph/0111134) [astro-ph]
- König O, Mastroserio G, Dauser T, et al (2024) Long term variability of Cygnus X-1. VIII. A spectral-timing look at low energies with NICER. *A&A* 687:A284. <https://doi.org/10.1051/0004-6361/202449333>, [arXiv:2405.07754](https://arxiv.org/abs/2405.07754) [astro-ph.HE]
- Körding E, Rupen M, Knigge C, et al (2008) A Transient Radio Jet in an Erupting Dwarf Nova. *Science* 320(5881):1318. <https://doi.org/10.1126/science.1155492>, [arXiv:0806.1002](https://arxiv.org/abs/0806.1002) [astro-ph]
- Krawczynski H, Beheshtipour B (2022) New Constraints on the Spin of the Black Hole Cygnus X-1 and the Physical Properties of its Accretion Disk Corona. *ApJ* 934(1):4. <https://doi.org/10.3847/1538-4357/ac7725>, [arXiv:2201.07360](https://arxiv.org/abs/2201.07360) [astro-ph.HE]
- Krawczynski H, Muleri F, Dovčiak M, et al (2022) Polarized x-rays constrain the disk-jet geometry in the black hole x-ray binary Cygnus X-1. *Science* 378(6620):650–654. <https://doi.org/10.1126/science.add5399>, [arXiv:2206.09972](https://arxiv.org/abs/2206.09972) [astro-ph.HE]
- Krawczynski H, Yuan Y, Chen AY, et al (2024) Evaluation of Several Explanations of the Strong X-Ray Polarization of the Black Hole X-Ray Binary 4U 1630-47. *ApJ* 977(1):L10. <https://doi.org/10.3847/2041-8213/ad855c>, [arXiv:2307.13141](https://arxiv.org/abs/2307.13141) [astro-ph.HE]
- Kubota A, Makishima K (2004) The Three Spectral Regimes Found in the Stellar Black Hole XTE J1550-564 in Its High/Soft State. *ApJ* 601(1):428–438. <https://doi.org/10.1086/380433>, [arXiv:astro-ph/0310085](https://arxiv.org/abs/astro-ph/0310085) [astro-ph]
- Kubota A, Makishima K, Ebisawa K (2001) Observational Evidence for Strong Disk Comptonization in GRO J1655-40. *ApJ* 560(2):L147–L150. <https://doi.org/10.1086/324377>, [arXiv:astro-ph/0105426](https://arxiv.org/abs/astro-ph/0105426) [astro-ph]

- Kushwaha A, Jayasurya KM, Agrawal VK, et al (2023) IXPE and NICER view of black hole X-ray binary 4U 1630-47: First significant detection of polarized emission in thermal state. *MNRAS* 524(1):L15–L20. <https://doi.org/10.1093/mnras/slad070>, [arXiv:2303.05462](https://arxiv.org/abs/2303.05462) [astro-ph.HE]
- Kylafis ND, Contopoulos I, Kazanas D, et al (2012) Formation and destruction of jets in X-ray binaries. *A&A* 538:A5. <https://doi.org/10.1051/0004-6361/201117052>
- Lamer G, Schwobe AD, Predehl P, et al (2021) A giant X-ray dust scattering ring discovered with SRG/eROSITA around the black hole transient MAXI J1348-630. *A&A* 647:A7. <https://doi.org/10.1051/0004-6361/202039757>, [arXiv:2012.11754](https://arxiv.org/abs/2012.11754) [astro-ph.HE]
- Laor A (1991) Line Profiles from a Disk around a Rotating Black Hole. *ApJ* 376:90. <https://doi.org/10.1086/170257>
- Lasota JP (2001) The disc instability model of dwarf novae and low-mass X-ray binary transients. *New A Rev.* 45(7):449–508. [https://doi.org/10.1016/S1387-6473\(01\)00112-9](https://doi.org/10.1016/S1387-6473(01)00112-9), [arXiv:astro-ph/0102072](https://arxiv.org/abs/astro-ph/0102072) [astro-ph]
- Liotine C, Zevin M, Berry CPL, et al (2023) The Missing Link between Black Holes in High-mass X-Ray Binaries and Gravitational-wave Sources: Observational Selection Effects. *ApJ* 946(1):4. <https://doi.org/10.3847/1538-4357/acb8b2>, [arXiv:2210.01825](https://arxiv.org/abs/2210.01825) [astro-ph.HE]
- Liu BF, Qiao E (2022) Accretion around black holes: The geometry and spectra. *iScience* 25(1):103544. <https://doi.org/10.1016/j.isci.2021.103544>, [arXiv:2201.06198](https://arxiv.org/abs/2201.06198) [astro-ph.HE]
- Liu BF, Meyer F, Meyer-Hofmeister E (2005) Spectral state transitions in low-mass X-ray binaries - the effect of hard and soft irradiation. *A&A* 442(2):555–562. <https://doi.org/10.1051/0004-6361:20053207>, [arXiv:astro-ph/0506444](https://arxiv.org/abs/astro-ph/0506444) [astro-ph]
- Liu H (2024) Probing the inner accretion flow around black holes with x-ray observations. PhD thesis, Fudan University
- Liu H, Zhou M, Bambi C (2018) Distinguishing black holes and naked singularities with iron line spectroscopy. *J. Cosmology Astropart. Phys.* 2018(8):044. <https://doi.org/10.1088/1475-7516/2018/08/044>, [arXiv:1801.00867](https://arxiv.org/abs/1801.00867) [gr-qc]
- Liu H, Abdikamalov AB, Ayzenberg D, et al (2019) Testing the Kerr hypothesis using x-ray reflection spectroscopy with NuSTAR data of Cygnus X-1 in the soft state. *Phys. Rev. D* 99(12):123007. <https://doi.org/10.1103/PhysRevD.99.123007>, [arXiv:1904.08027](https://arxiv.org/abs/1904.08027) [gr-qc]
- Liu H, Ji L, Bambi C, et al (2021) Testing Evolution of LFQPOs with Mass Accretion Rate in GRS 1915+105 with Insight-HXMT. *ApJ* 909(1):63. <https://doi.org/10.3847/1538-4357/abf8b2>

[3847/1538-4357/abdf65](#), [arXiv:2012.01825](#) [astro-ph.HE]

- Liu H, Bambi C, Jiang J, et al (2023a) The Hard-to-soft Transition of GX 339-4 as Seen by Insight-HXMT. *ApJ* 950(1):5. <https://doi.org/10.3847/1538-4357/acca17>, [arXiv:2211.09543](#) [astro-ph.HE]
- Liu H, Jiang J, Zhang Z, et al (2023b) High-density Reflection Spectroscopy of Black Hole X-Ray Binaries in the Hard State. *ApJ* 951(2):145. <https://doi.org/10.3847/1538-4357/acd8b9>, [arXiv:2303.10593](#) [astro-ph.HE]
- Liu H, Abdikamalov AB, Mirzaev T, et al (2025) About the accuracy of the `relxill/relxill_nk` models in view of the next generation of X-ray missions. *MNRAS* 536(3):2594–2602. <https://doi.org/10.1093/mnras/stae2722>, [arXiv:2412.00349](#) [astro-ph.HE]
- Lucchini M, Mastroserio G, Wang J, et al (2023) Investigating the Impact of Vertically Extended Coronae on X-Ray Reverberation Mapping. *ApJ* 951(1):19. <https://doi.org/10.3847/1538-4357/acd24f>, [arXiv:2305.05039](#) [astro-ph.HE]
- Lyubarskii YE (1997) Flicker noise in accretion discs. *MNRAS* 292(3):679–685. <https://doi.org/10.1093/mnras/292.3.679>
- Ma R, Méndez M, García F, et al (2023) A variable corona during the transition from type-C to type-B quasi-periodic oscillations in the black hole X-ray binary MAXI J1820+070. *MNRAS* 525(1):854–875. <https://doi.org/10.1093/mnras/stad2284>, [arXiv:2307.12728](#) [astro-ph.HE]
- Ma X, Tao L, Zhang SN, et al (2021) Discovery of oscillations above 200 keV in a black hole X-ray binary with Insight-HXMT. *Nature Astronomy* 5:94–102. <https://doi.org/10.1038/s41550-020-1192-2>, [arXiv:2009.10607](#) [astro-ph.HE]
- Magdziarz P, Zdziarski AA (1995) Angle-dependent Compton reflection of X-rays and gamma-rays. *MNRAS* 273(3):837–848. <https://doi.org/10.1093/mnras/273.3.837>
- Malzac J, Belmont R (2009) The synchrotron boiler and the spectral states of black hole binaries. *MNRAS* 392(2):570–589. <https://doi.org/10.1111/j.1365-2966.2008.14142.x>, [arXiv:0810.4458](#) [astro-ph]
- Malzac J, Beloborodov AM, Poutanen J (2001) X-ray spectra of accretion discs with dynamic coronae. *MNRAS* 326(2):417–427. <https://doi.org/10.1046/j.1365-8711.2001.04450.x>, [arXiv:astro-ph/0102490](#) [astro-ph]
- Marin F (2018) Modeling optical and UV polarization of AGNs. V. Dilution by interstellar polarization and the host galaxy. *A&A* 615:A171. <https://doi.org/10.1051/0004-6361/201833225>, [arXiv:1805.09098](#) [astro-ph.HE]
- Markoff S, Nowak MA, Wilms J (2005) Going with the Flow: Can the Base of Jets Subsume the Role of Compact Accretion Disk Coronae? *ApJ* 635(2):1203–1216.

- <https://doi.org/10.1086/497628>, [arXiv:astro-ph/0509028](https://arxiv.org/abs/astro-ph/0509028) [astro-ph]
- Marra L, Brigitte M, Rodriguez Cavero N, et al (2024) IXPE observation confirms a high spin in the accreting black hole 4U 1957+115. *A&A* 684:A95. <https://doi.org/10.1051/0004-6361/202348277>, [arXiv:2310.11125](https://arxiv.org/abs/2310.11125) [astro-ph.HE]
- Mastroserio G, Ingram A, van der Klis M (2020) Multi-timescale reverberation mapping of Mrk 335. *MNRAS* 498(4):4971–4982. <https://doi.org/10.1093/mnras/staa2735>, [arXiv:2009.03908](https://arxiv.org/abs/2009.03908) [astro-ph.HE]
- Mastroserio G, De Marco B, Baglio MC, et al (2025) X-Ray and Optical Polarization Aligned with the Radio Jet Ejecta in GX 339–4. *ApJ* 978(2):L19. <https://doi.org/10.3847/2041-8213/ad9913>, [arXiv:2408.06856](https://arxiv.org/abs/2408.06856) [astro-ph.HE]
- Matt G (1993) X-ray polarization properties of a centrally illuminated accretion disc. *MNRAS* 260:663–674. <https://doi.org/10.1093/mnras/260.3.663>
- McClintock JE, Remillard RA (2006) Black hole binaries. In: Lewin W, van der Klis M (eds) *Compact stellar X-ray sources*, Cambridge Astrophysics Series, vol 39. Cambridge University Press, Cambridge, p 157–213, <https://doi.org/10.48550/arXiv.astro-ph/0306213>
- McClintock JE, Narayan R, Steiner JF (2014) Black Hole Spin via Continuum Fitting and the Role of Spin in Powering Transient Jets. *Space Sci. Rev.* 183(1-4):295–322. <https://doi.org/10.1007/s11214-013-0003-9>, [arXiv:1303.1583](https://arxiv.org/abs/1303.1583) [astro-ph.HE]
- McConnell ML, Zdziarski AA, Bennett K, et al (2002) The Soft Gamma-Ray Spectral Variability of Cygnus X-1. *ApJ* 572(2):984–995. <https://doi.org/10.1086/340436>, [arXiv:astro-ph/0112326](https://arxiv.org/abs/astro-ph/0112326) [astro-ph]
- McHardy IM, Koeding E, Knigge C, et al (2006) Active galactic nuclei as scaled-up Galactic black holes. *Nature* 444(7120):730–732. <https://doi.org/10.1038/nature05389>, [arXiv:astro-ph/0612273](https://arxiv.org/abs/astro-ph/0612273) [astro-ph]
- Méndez M, Karpouzas K, García F, et al (2022) Coupling between the accreting corona and the relativistic jet in the microquasar GRS 1915+105. *Nature Astronomy* 6:577–583. <https://doi.org/10.1038/s41550-022-01617-y>, [arXiv:2203.02963](https://arxiv.org/abs/2203.02963) [astro-ph.HE]
- Merloni A, Fabian AC, Ross RR (2000) On the interpretation of the multicolour disc model for black hole candidates. *MNRAS* 313(1):193–197. <https://doi.org/10.1046/j.1365-8711.2000.03226.x>, [arXiv:astro-ph/9911457](https://arxiv.org/abs/astro-ph/9911457) [astro-ph]
- Meyer-Hofmeister E, Liu BF, Meyer F (2005) Hysteresis in spectral state transitions - a challenge for theoretical modeling. *A&A* 432(1):181–187. <https://doi.org/10.1051/0004-6361:20041631>, [arXiv:astro-ph/0411145](https://arxiv.org/abs/astro-ph/0411145) [astro-ph]

- Mikusincova R, Dovciak M, Bursa M, et al (2023) X-ray polarimetry as a tool to measure the black hole spin in microquasars: simulations of IXPE capabilities. *MNRAS* 519(4):6138–6148. <https://doi.org/10.1093/mnras/stad077>, [arXiv:2301.04002](https://arxiv.org/abs/2301.04002) [astro-ph.HE]
- Miller JM, Fabian AC, Wijnands R, et al (2002) Evidence of Spin and Energy Extraction in a Galactic Black Hole Candidate: The XMM-Newton/EPIC-pn Spectrum of XTE J1650-500. *ApJ* 570(2):L69–L73. <https://doi.org/10.1086/341099>, [arXiv:astro-ph/0202375](https://arxiv.org/abs/astro-ph/0202375) [astro-ph]
- Miller JM, Fabian AC, Reynolds CS, et al (2004) Evidence of Black Hole Spin in GX 339-4: XMM-Newton/EPIC-pn and RXTE Spectroscopy of the Very High State. *ApJ* 606(2):L131–L134. <https://doi.org/10.1086/421263>, [arXiv:astro-ph/0312033](https://arxiv.org/abs/astro-ph/0312033) [astro-ph]
- Miller-Jones JCA, Sivakoff GR, Altamirano D, et al (2012) Disc-jet coupling in the 2009 outburst of the black hole candidate H1743-322. *MNRAS* 421(1):468–485. <https://doi.org/10.1111/j.1365-2966.2011.20326.x>, [arXiv:1201.1678](https://arxiv.org/abs/1201.1678) [astro-ph.HE]
- Miniutti G, Fabian AC (2004) A light bending model for the X-ray temporal and spectral properties of accreting black holes. *MNRAS* 349(4):1435–1448. <https://doi.org/10.1111/j.1365-2966.2004.07611.x>, [arXiv:astro-ph/0309064](https://arxiv.org/abs/astro-ph/0309064) [astro-ph]
- Mirzaev T, Bambi C, Abdikamalov AB, et al (2024a) X-Ray Spectra of Black Hole X-Ray Binaries with Returning Radiation. *ApJ* 976(2):229. <https://doi.org/10.3847/1538-4357/ad8a63>, [arXiv:2406.01226](https://arxiv.org/abs/2406.01226) [astro-ph.HE]
- Mirzaev T, Riaz S, Abdikamalov AB, et al (2024b) Toward More Accurate Synthetic Reflection Spectra: Improving the Calculations of Returning Radiation. *ApJ* 965(1):66. <https://doi.org/10.3847/1538-4357/ad303b>, [arXiv:2401.05582](https://arxiv.org/abs/2401.05582) [astro-ph.HE]
- Mitsuda K, Inoue H, Koyama K, et al (1984) Energy spectra of low-mass binary X-ray sources observed from Tenma. *PASJ* 36:741–759
- Motta S, Muñoz-Darias T, Casella P, et al (2011) Low-frequency oscillations in black holes: a spectral-timing approach to the case of GX 339-4. *MNRAS* 418(4):2292–2307. <https://doi.org/10.1111/j.1365-2966.2011.19566.x>, [arXiv:1108.0540](https://arxiv.org/abs/1108.0540) [astro-ph.HE]
- Motta SE, Belloni TM, Stella L, et al (2014) Precise mass and spin measurements for a stellar-mass black hole through X-ray timing: the case of GRO J1655-40. *MNRAS* 437(3):2554–2565. <https://doi.org/10.1093/mnras/stt2068>, [arXiv:1309.3652](https://arxiv.org/abs/1309.3652) [astro-ph.HE]
- Muñoz-Darias T, Motta S, Belloni TM (2011) Fast variability as a tracer of accretion regimes in black hole transients. *MNRAS* 410(1):679–684. <https://doi.org/10.1111/>

- [j.1365-2966.2010.17476.x](#), [arXiv:1008.0558](#) [astro-ph.HE]
- Mummery A, Stone JM (2024) The three-dimensional structure of black hole accretion flows within the plunging region. *MNRAS* 532(3):3395–3416. <https://doi.org/10.1093/mnras/stae1643>, [arXiv:2407.02164](#) [astro-ph.HE]
- Mummery A, Ingram A, Davis S, et al (2024a) Continuum emission from within the plunging region of black hole discs. *MNRAS* 531(1):366–386. <https://doi.org/10.1093/mnras/stae1160>, [arXiv:2405.09175](#) [astro-ph.HE]
- Mummery A, Jiang J, Fabian A (2024b) Plunging region emission in the X-ray binary MAXI J0637-430. *MNRAS* 533(1):L83–L90. <https://doi.org/10.1093/mnras/slae056>, [arXiv:2406.14957](#) [astro-ph.HE]
- Murdin P, Webster BL (1971) Optical Identification of Cygnus X-1. *Nature* 233(5315):110. <https://doi.org/10.1038/233110a0>
- Nandra K, O’Neill PM, George IM, et al (2007) An XMM-Newton survey of broad iron lines in Seyfert galaxies. *MNRAS* 382(1):194–228. <https://doi.org/10.1111/j.1365-2966.2007.12331.x>, [arXiv:0708.1305](#) [astro-ph]
- Narayan R, Yi I (1994) Advection-dominated Accretion: A Self-similar Solution. *ApJ* 428:L13. <https://doi.org/10.1086/187381>, [arXiv:astro-ph/9403052](#) [astro-ph]
- Nathan E, Ingram A, Steiner JF, et al (2024) Proof of principle X-ray reflection mass measurement of the black hole in H1743-322. *MNRAS* 533(2):2441–2453. <https://doi.org/10.1093/mnras/stae1896>, [arXiv:2408.05268](#) [astro-ph.HE]
- Nayakshin S, Kazanas D, Kallman TR (2000) Thermal Instability and Photoionized X-Ray Reflection in Accretion Disks. *ApJ* 537(2):833–852. <https://doi.org/10.1086/309054>, [arXiv:astro-ph/9909359](#) [astro-ph]
- Nekrasov AD, Dauser T, García JA, et al (2025) Relativistic reflection within an extended hot plasma geometry. *A&A* 704:A129. <https://doi.org/10.1051/0004-6361/202556012>, [arXiv:2510.13337](#) [astro-ph.HE]
- Neumann M, Avakyan A, Doroshenko V, et al (2023) XRBcats: Galactic High Mass X-ray Binary Catalogue. *A&A* 677:A134. <https://doi.org/10.1051/0004-6361/202245728>, [arXiv:2303.16137](#) [astro-ph.HE]
- Nitindala AP, Veledina A, Poutanen J (2025) X-ray polarization from accretion disk winds. *A&A* 694:A230. <https://doi.org/10.1051/0004-6361/202453188>, [arXiv:2411.18299](#) [astro-ph.HE]
- Novikov ID, Thorne KS (1973) Astrophysics of black holes. In: Dewitt C, Dewitt BS (eds) *Black Holes (Les Astres Occlus)*, pp 343–450

- Nowak MA, Hanke M, Trowbridge SN, et al (2011) Corona, Jet, and Relativistic Line Models for Suzaku/RXTE/Chandra-HETG Observations of the Cygnus X-1 Hard State. *ApJ* 728(1):13. <https://doi.org/10.1088/0004-637X/728/1/13>, [arXiv:1012.4801](https://arxiv.org/abs/1012.4801) [astro-ph.HE]
- Nowak MA, Wilms J, Pottschmidt K, et al (2012) Suzaku Observations of 4U 1957+11: Potentially the Most Rapidly Spinning Black Hole in (the Halo of) the Galaxy. *ApJ* 744(2):107. <https://doi.org/10.1088/0004-637X/744/2/107>, [arXiv:1109.6008](https://arxiv.org/abs/1109.6008) [astro-ph.HE]
- Parker ML, Tomsick JA, Kennea JA, et al (2016) NuSTAR and Swift Observations of the Very High State in GX 339-4: Weighing the Black Hole with X-Rays. *ApJ* 821(1):L6. <https://doi.org/10.3847/2041-8205/821/1/L6>, [arXiv:1603.03777](https://arxiv.org/abs/1603.03777) [astro-ph.HE]
- Parker ML, Buisson DJK, Tomsick JA, et al (2019) XRB continuum fitting with sensitive high-energy X-ray detectors. *MNRAS* 484(1):1202–1212. <https://doi.org/10.1093/mnras/stz045>, [arXiv:1901.00683](https://arxiv.org/abs/1901.00683) [astro-ph.HE]
- Peirano V, Méndez M, García F, et al (2023) Dual-corona Comptonization model for the type-b quasi-periodic oscillations in GX 339-4. *MNRAS* 519(1):1336–1348. <https://doi.org/10.1093/mnras/stac3553>, [arXiv:2212.00062](https://arxiv.org/abs/2212.00062) [astro-ph.HE]
- Petrucci PO, Ferreira J, Henri G, et al (2008) The role of the disc magnetization on the hysteresis behaviour of X-ray binaries. *MNRAS* 385(1):L88–L92. <https://doi.org/10.1111/j.1745-3933.2008.00439.x>, [arXiv:0712.3388](https://arxiv.org/abs/0712.3388) [astro-ph]
- Petrucci PO, Cabanac C, Corbel S, et al (2014) The return to the hard state of GX 339-4 as seen by Suzaku. *A&A* 564:A37. <https://doi.org/10.1051/0004-6361/201322268>, [arXiv:1310.3039](https://arxiv.org/abs/1310.3039) [astro-ph.HE]
- Plotkin RM, Gallo E, Jonker PG (2013) The X-Ray Spectral Evolution of Galactic Black Hole X-Ray Binaries toward Quiescence. *ApJ* 773(1):59. <https://doi.org/10.1088/0004-637X/773/1/59>, [arXiv:1306.1570](https://arxiv.org/abs/1306.1570) [astro-ph.HE]
- Podgorný J, Dovčiak M, Marin F, et al (2022) Spectral and polarization properties of reflected X-ray emission from black hole accretion discs. *MNRAS* 510(4):4723–4735. <https://doi.org/10.1093/mnras/stab3714>, [arXiv:2201.07494](https://arxiv.org/abs/2201.07494) [astro-ph.HE]
- Podgorný J, Dovčiak M, Goosmann R, et al (2023) Spectral and polarization properties of reflected X-ray emission from black-hole accretion discs for a distant observer: the lamp-post model. *MNRAS* 524(3):3853–3876. <https://doi.org/10.1093/mnras/stad2169>, [arXiv:2307.08819](https://arxiv.org/abs/2307.08819) [astro-ph.HE]
- Podgorný J, Svoboda J, Dovčiak M, et al (2024) Recovery of the X-ray polarisation of Swift J1727.8–1613 after the soft-to-hard spectral transition. *A&A* 686:L12. <https://doi.org/10.1051/0004-6361/202450566>, [arXiv:2404.19601](https://arxiv.org/abs/2404.19601) [astro-ph.HE]

- Poutanen J, Svensson R (1996) The Two-Phase Pair Corona Model for Active Galactic Nuclei and X-Ray Binaries: How to Obtain Exact Solutions. *ApJ* 470:249. <https://doi.org/10.1086/177865>, [arXiv:astro-ph/9605073](https://arxiv.org/abs/astro-ph/9605073) [astro-ph]
- Poutanen J, Vurm I (2009) On the Origin of Spectral States in Accreting Black Holes. *ApJ* 690(2):L97–L100. <https://doi.org/10.1088/0004-637X/690/2/L97>, [arXiv:0807.3073](https://arxiv.org/abs/0807.3073) [astro-ph]
- Poutanen J, Veledina A, Zdziarski AA (2018) Doughnut strikes sandwich: the geometry of hot medium in accreting black hole X-ray binaries. *A&A* 614:A79. <https://doi.org/10.1051/0004-6361/201732345>, [arXiv:1711.08509](https://arxiv.org/abs/1711.08509) [astro-ph.HE]
- Poutanen J, Veledina A, Beloborodov AM (2023) Polarized X-Rays from Windy Accretion in Cygnus X-1. *ApJ* 949(1):L10. <https://doi.org/10.3847/2041-8213/acd33e>, [arXiv:2302.11674](https://arxiv.org/abs/2302.11674) [astro-ph.HE]
- Punsly B, Rodriguez J (2013) The Relationship between X-Ray Luminosity and Major Flare Launching in GRS 1915+105. *ApJ* 764(2):173. <https://doi.org/10.1088/0004-637X/764/2/173>, [arXiv:1212.0450](https://arxiv.org/abs/1212.0450) [astro-ph.HE]
- Ratheesh A, Dovčiak M, Krawczynski H, et al (2024) X-Ray Polarization of the Black Hole X-Ray Binary 4U 1630–47 Challenges the Standard Thin Accretion Disk Scenario. *ApJ* 964(1):77. <https://doi.org/10.3847/1538-4357/ad226e>, [arXiv:2304.12752](https://arxiv.org/abs/2304.12752) [astro-ph.HE]
- Reis RC, Miller JM (2013) On the Size and Location of the X-Ray Emitting Coronae around Black Holes. *ApJ* 769(1):L7. <https://doi.org/10.1088/2041-8205/769/1/L7>, [arXiv:1304.4947](https://arxiv.org/abs/1304.4947) [astro-ph.HE]
- Reis RC, Fabian AC, Ross RR, et al (2008) A systematic look at the very high and low/hard state of GX339-4: constraining the black hole spin with a new reflection model. *MNRAS* 387(4):1489–1498. <https://doi.org/10.1111/j.1365-2966.2008.13358.x>, [arXiv:0804.0238](https://arxiv.org/abs/0804.0238) [astro-ph]
- Reis RC, Fabian AC, Ross RR, et al (2009) Determining the spin of two stellar-mass black holes from disc reflection signatures. *MNRAS* 395(3):1257–1264. <https://doi.org/10.1111/j.1365-2966.2009.14622.x>
- Reis RC, Miller JM, Fabian AC, et al (2011) Multistate observations of the Galactic black hole XTE J1752-223: evidence for an intermediate black hole spin. *MNRAS* 410(4):2497–2505. <https://doi.org/10.1111/j.1365-2966.2010.17628.x>, [arXiv:1009.1154](https://arxiv.org/abs/1009.1154) [astro-ph.HE]
- Reis RC, Miller JM, Reynolds MT, et al (2012) Suzaku Observation of the Black Hole Candidate Maxi J1836-194 in a Hard/Intermediate Spectral State. *ApJ* 751(1):34. <https://doi.org/10.1088/0004-637X/751/1/34>, [arXiv:1111.6665](https://arxiv.org/abs/1111.6665) [astro-ph.HE]

- Reis RC, Reynolds MT, Miller JM, et al (2013) SWIFT J1910.2-0546: A Possible Black Hole Binary with a Retrograde Spin or Truncated Disk. *ApJ* 778(2):155. <https://doi.org/10.1088/0004-637X/778/2/155>, [arXiv:1310.0417](https://arxiv.org/abs/1310.0417) [astro-ph.HE]
- Remillard RA, McClintock JE (2006) X-Ray Properties of Black-Hole Binaries. *ARA&A* 44(1):49–92. <https://doi.org/10.1146/annurev.astro.44.051905.092532>, [arXiv:astro-ph/0606352](https://arxiv.org/abs/astro-ph/0606352) [astro-ph]
- Ren XQ, Wang Y, Zhang SN, et al (2022) Insight-HXMT Study of the Inner Accretion Disk in the Black Hole Candidate EXO 1846-031. *ApJ* 932(1):66. <https://doi.org/10.3847/1538-4357/ac6dd7>, [arXiv:2205.04635](https://arxiv.org/abs/2205.04635) [astro-ph.HE]
- Reynolds CS (2021) Observational Constraints on Black Hole Spin. *ARA&A* 59:117–154. <https://doi.org/10.1146/annurev-astro-112420-035022>, [arXiv:2011.08948](https://arxiv.org/abs/2011.08948) [astro-ph.HE]
- Reynolds MT, Reis RC, Miller JM, et al (2014) The quiescent X-ray spectrum of accreting black holes. *MNRAS* 441(4):3656–3665. <https://doi.org/10.1093/mnras/stu832>, [arXiv:1405.0474](https://arxiv.org/abs/1405.0474) [astro-ph.HE]
- Riaz S, Ayzenberg D, Bambi C, et al (2020a) Modeling Bias in Supermassive Black Hole Spin Measurements. *ApJ* 895(1):61. <https://doi.org/10.3847/1538-4357/ab89ab>, [arXiv:1911.06605](https://arxiv.org/abs/1911.06605) [astro-ph.HE]
- Riaz S, Ayzenberg D, Bambi C, et al (2020b) Reflection spectra of thick accretion discs. *MNRAS* 491(1):417–426. <https://doi.org/10.1093/mnras/stz3022>, [arXiv:1908.04969](https://arxiv.org/abs/1908.04969) [astro-ph.HE]
- Riaz S, Abdikamalov AB, Ayzenberg D, et al (2022) Reflection Spectra of Accretion Disks Illuminated by Disk-like Coronae. *ApJ* 925(1):51. <https://doi.org/10.3847/1538-4357/ac3827>
- Rodriguez J, Corbel S, Caballero I, et al (2011) First simultaneous multi-wavelength observations of the black hole candidate IGR J17091-3624. ATCA, INTEGRAL, Swift, and RXTE views of the 2011 outburst. *A&A* 533:L4. <https://doi.org/10.1051/0004-6361/201117511>, [arXiv:1108.0666](https://arxiv.org/abs/1108.0666) [astro-ph.HE]
- Ross RR, Fabian AC (2005) A comprehensive range of X-ray ionized-reflection models. *MNRAS* 358(1):211–216. <https://doi.org/10.1111/j.1365-2966.2005.08797.x>, [arXiv:astro-ph/0501116](https://arxiv.org/abs/astro-ph/0501116) [astro-ph]
- Ross RR, Fabian AC (2007) X-ray reflection in accreting stellar-mass black hole systems. *MNRAS* 381(4):1697–1701. <https://doi.org/10.1111/j.1365-2966.2007.12339.x>, [arXiv:0709.0270](https://arxiv.org/abs/0709.0270) [astro-ph]
- Russell DM, Shahbaz T (2014) The multiwavelength polarization of Cygnus X-1. *MNRAS* 438(3):2083–2096. <https://doi.org/10.1093/mnras/stt2330>,

[arXiv:1312.0942](#) [astro-ph.HE]

- Russell TD, Tetarenko AJ, Miller-Jones JCA, et al (2019) Disk-Jet Coupling in the 2017/2018 Outburst of the Galactic Black Hole Candidate X-Ray Binary MAXI J1535-571. *ApJ* 883(2):198. <https://doi.org/10.3847/1538-4357/ab3d36>, [arXiv:1906.00998](#) [astro-ph.HE]
- Salvesen G (2022) An Electron-scattering Time Delay in Black Hole Accretion Disks. *ApJ* 940(1):L22. <https://doi.org/10.3847/2041-8213/ac9cdd>, [arXiv:2209.14304](#) [astro-ph.HE]
- Schnittman JD, Krolik JH (2010) X-ray Polarization from Accreting Black Holes: Coronal Emission. *ApJ* 712(2):908–924. <https://doi.org/10.1088/0004-637X/712/2/908>, [arXiv:0912.0907](#) [astro-ph.HE]
- Shakura NI, Sunyaev RA (1973) Black holes in binary systems. Observational appearance. *A&A* 24:337–355
- Shapiro SL, Lightman AP, Eardley DM (1976) A two-temperature accretion disk model for Cygnus X-1: structure and spectrum. *ApJ* 204:187–199. <https://doi.org/10.1086/154162>
- Shashank S, Liu H, Abdikamalov AB, et al (2024) Modeling reflection spectra of super-Eddington X-ray sources. arXiv e-prints [arXiv:2407.12890](#). <https://doi.org/10.48550/arXiv.2407.12890>, [arXiv:2407.12890](#) [astro-ph.HE]
- Shidatsu M, Ueda Y, Tazaki F, et al (2011) X-Ray and Near-Infrared Observations of GX 339-4 in the Low/Hard State with Suzaku and IRSF. *PASJ* 63:S785–S801. <https://doi.org/10.1093/pasj/63.sp3.S785>, [arXiv:1105.3586](#) [astro-ph.HE]
- Shimura T, Takahara F (1995) On the Spectral Hardening Factor of the X-Ray Emission from Accretion Disks in Black Hole Candidates. *ApJ* 445:780. <https://doi.org/10.1086/175740>
- Smith DM, Dawson DM, Swank JH (2007) Hysteresis of Spectral Evolution in the Soft State of Black Hole Binary LMC X-3. *ApJ* 669(2):1138–1142. <https://doi.org/10.1086/521822>, [arXiv:0707.3154](#) [astro-ph]
- Sobolewska MA, Papadakis IE, Done C, et al (2011) Evidence for a change in the X-ray radiation mechanism in the hard state of Galactic black holes. *MNRAS* 417(1):280–288. <https://doi.org/10.1111/j.1365-2966.2011.19209.x>, [arXiv:1106.1645](#) [astro-ph.HE]
- Sridhar N, Bhattacharyya S, Chandra S, et al (2019) Broad-band reflection spectroscopy of MAXI J1535-571 using AstroSat: estimation of black hole mass and spin. *MNRAS* 487(3):4221–4229. <https://doi.org/10.1093/mnras/stz1476>, [arXiv:1905.09253](#) [astro-ph.HE]

- Sridhar N, García JA, Steiner JF, et al (2020) Evolution of the Accretion Disk-Corona during the Bright Hard-to-soft State Transition: A Reflection Spectroscopic Study with GX 339-4. *ApJ* 890(1):53. <https://doi.org/10.3847/1538-4357/ab64f5>, [arXiv:1912.11447](https://arxiv.org/abs/1912.11447) [astro-ph.HE]
- Sridhar N, Sironi L, Beloborodov AM (2023) Comptonization by reconnection plasmoids in black hole coronae II: Electron-ion plasma. *MNRAS* 518(1):1301–1315. <https://doi.org/10.1093/mnras/stac2730>, [arXiv:2203.02856](https://arxiv.org/abs/2203.02856) [astro-ph.HE]
- Steiner JF, McClintock JE, Remillard RA, et al (2010) The Constant Inner-disk Radius of LMC X-3: A Basis for Measuring Black Hole Spin. *ApJ* 718(2):L117–L121. <https://doi.org/10.1088/2041-8205/718/2/L117>, [arXiv:1006.5729](https://arxiv.org/abs/1006.5729) [astro-ph.HE]
- Steiner JF, Reis RC, McClintock JE, et al (2011) The spin of the black hole microquasar XTE J1550-564 via the continuum-fitting and Fe-line methods. *MNRAS* 416(2):941–958. <https://doi.org/10.1111/j.1365-2966.2011.19089.x>, [arXiv:1010.1013](https://arxiv.org/abs/1010.1013) [astro-ph.HE]
- Steiner JF, McClintock JE, Reid MJ (2012a) The Distance, Inclination, and Spin of the Black Hole Microquasar H1743-322. *ApJ* 745(1):L7. <https://doi.org/10.1088/2041-8205/745/1/L7>, [arXiv:1111.2388](https://arxiv.org/abs/1111.2388) [astro-ph.HE]
- Steiner JF, Reis RC, Fabian AC, et al (2012b) A broad iron line in LMC X-1. *MNRAS* 427(3):2552–2561. <https://doi.org/10.1111/j.1365-2966.2012.22128.x>, [arXiv:1209.3269](https://arxiv.org/abs/1209.3269) [astro-ph.HE]
- Steiner JF, McClintock JE, Orosz JA, et al (2014) The Low-spin Black Hole in LMC X-3. *ApJ* 793(2):L29. <https://doi.org/10.1088/2041-8205/793/2/L29>, [arXiv:1402.0148](https://arxiv.org/abs/1402.0148) [astro-ph.HE]
- Steiner JF, Remillard RA, García JA, et al (2016) Stronger Reflection from Black Hole Accretion Disks in Soft X-Ray States. *ApJ* 829(2):L22. <https://doi.org/10.3847/2041-8205/829/2/L22>, [arXiv:1609.04592](https://arxiv.org/abs/1609.04592) [astro-ph.HE]
- Steiner JF, Nathan E, Hu K, et al (2024) An IXPE-led X-Ray Spectropolarimetric Campaign on the Soft State of Cygnus X-1: X-Ray Polarimetric Evidence for Strong Gravitational Lensing. *ApJ* 969(2):L30. <https://doi.org/10.3847/2041-8213/ad58e4>, [arXiv:2406.12014](https://arxiv.org/abs/2406.12014) [astro-ph.HE]
- Stern BE, Poutanen J, Svensson R, et al (1995) On the Geometry of the X-Ray-Emitting Region in Seyfert Galaxies. *ApJ* 449:L13. <https://doi.org/10.1086/309617>, [arXiv:astro-ph/9506035](https://arxiv.org/abs/astro-ph/9506035) [astro-ph]
- Svoboda J, Dovčiak M, Steiner JF, et al (2024a) Dramatic Drop in the X-Ray Polarization of Swift J1727.8–1613 in the Soft Spectral State. *ApJ* 966(2):L35. <https://doi.org/10.3847/2041-8213/ad402e>, [arXiv:2403.04689](https://arxiv.org/abs/2403.04689) [astro-ph.HE]

- Svoboda J, Dovčiak M, Steiner JF, et al (2024b) First X-Ray Polarization Measurement Confirms the Low Black Hole Spin in LMC X-3. *ApJ* 960(1):3. <https://doi.org/10.3847/1538-4357/ad0842>, [arXiv:2309.10813](https://arxiv.org/abs/2309.10813) [astro-ph.HE]
- Tagger M, Pellat R (1999) An accretion-ejection instability in magnetized disks. *A&A* 349:1003–1016. <https://doi.org/10.48550/arXiv.astro-ph/9907267>, [arXiv:astro-ph/9907267](https://arxiv.org/abs/astro-ph/9907267) [astro-ph]
- Tanaka Y, Lewin WHG (1995) Black hole binaries. In: Lewin WHG, van Paradijs J, van den Heuvel EPJ (eds) *X-ray Binaries*, pp 126–174
- Tao L, Tomsick JA, Qu J, et al (2019) The Spin of the Black Hole GRS 1716-249 Determined from the Hard Intermediate State. *ApJ* 887(2):184. <https://doi.org/10.3847/1538-4357/ab5282>, [arXiv:1910.11979](https://arxiv.org/abs/1910.11979) [astro-ph.HE]
- Tashiro M, Maejima H, Toda K, et al (2020) Status of x-ray imaging and spectroscopy mission (XRISM). In: den Herder JWA, Nikzad S, Nakazawa K (eds) *Space Telescopes and Instrumentation 2020: Ultraviolet to Gamma Ray*, p 1144422, <https://doi.org/10.1117/12.2565812>
- Taverna R, Zhang W, Dovčiak M, et al (2020) Towards a complete description of spectra and polarization of black hole accretion discs: albedo profiles and returning radiation. *MNRAS* 493(4):4960–4977. <https://doi.org/10.1093/mnras/staa598>, [arXiv:2002.11788](https://arxiv.org/abs/2002.11788) [astro-ph.HE]
- Taverna R, Marra L, Bianchi S, et al (2021) Spectral and polarization properties of black hole accretion disc emission: including absorption effects. *MNRAS* 501(3):3393–3405. <https://doi.org/10.1093/mnras/staa3859>, [arXiv:2012.06504](https://arxiv.org/abs/2012.06504) [astro-ph.HE]
- Taylor C, Reynolds CS (2018) Exploring the Effects of Disk Thickness on the Black Hole Reflection Spectrum. *ApJ* 855(2):120. <https://doi.org/10.3847/1538-4357/aaad63>, [arXiv:1712.05418](https://arxiv.org/abs/1712.05418) [astro-ph.HE]
- Tetarenko BE, Sivakoff GR, Heinke CO, et al (2016) WATCHDOG: A Comprehensive All-sky Database of Galactic Black Hole X-ray Binaries. *ApJS* 222(2):15. <https://doi.org/10.3847/0067-0049/222/2/15>, [arXiv:1512.00778](https://arxiv.org/abs/1512.00778) [astro-ph.HE]
- Thomsen LL, Lixin Dai J, Ramirez-Ruiz E, et al (2019) X-Ray Fluorescence from Super-Eddington Accreting Black Holes. *ApJ* 884(1):L21. <https://doi.org/10.3847/2041-8213/ab4518>, [arXiv:1907.11462](https://arxiv.org/abs/1907.11462) [astro-ph.GA]
- Thorne KS, Price RH (1975) Cygnus X-1: an interpretation of the spectrum and its variability. *ApJ* 195:L101–L105. <https://doi.org/10.1086/181720>
- Tomsick JA, Kalemci E, Kaaret P, et al (2008) Broadband X-Ray Spectra of GX 339-4 and the Geometry of Accreting Black Holes in the Hard State. *ApJ* 680(1):593–601.

- <https://doi.org/10.1086/587797>, [arXiv:0802.3357](https://arxiv.org/abs/0802.3357) [astro-ph]
- Tomsick JA, Yamaoka K, Corbel S, et al (2009) Truncation of the Inner Accretion Disk Around a Black Hole at Low Luminosity. *ApJ* 707(1):L87–L91. <https://doi.org/10.1088/0004-637X/707/1/L87>, [arXiv:0911.2240](https://arxiv.org/abs/0911.2240) [astro-ph.HE]
- Tripathi A, Abdikamalov AB, Ayzenberg D, et al (2021) Impact of the Disk Thickness on X-Ray Reflection Spectroscopy Measurements. *ApJ* 913(2):129. <https://doi.org/10.3847/1538-4357/abf6c5>, [arXiv:2102.04695](https://arxiv.org/abs/2102.04695) [astro-ph.HE]
- Ursini F, Matt G, Bianchi S, et al (2022) Prospects for differentiating extended coronal geometries in AGNs with the IXPE mission. *MNRAS* 510(3):3674–3687. <https://doi.org/10.1093/mnras/stab3745>, [arXiv:2112.11268](https://arxiv.org/abs/2112.11268) [astro-ph.HE]
- Uttley P, Cackett EM, Fabian AC, et al (2014) X-ray reverberation around accreting black holes. *A&A Rev.* 22:72. <https://doi.org/10.1007/s00159-014-0072-0>, [arXiv:1405.6575](https://arxiv.org/abs/1405.6575) [astro-ph.HE]
- Vadawale SV, Rao AR, Naik S, et al (2003) On the Origin of the Various Types of Radio Emission in GRS 1915+105. *ApJ* 597(2):1023–1035. <https://doi.org/10.1086/378672>, [arXiv:astro-ph/0308096](https://arxiv.org/abs/astro-ph/0308096) [astro-ph]
- van der Klis M (1989) Fourier techniques in X-ray timing. In: Ögelman H, van den Heuvel EPJ (eds) *Timing Neutron Stars*, p 27, [https://doi.org/10.1007/978-94-009-2273-0\\_3](https://doi.org/10.1007/978-94-009-2273-0_3)
- Varnière P, Tagger M (2002) Accretion-Ejection Instability in magnetized disks: Feeding the corona with Alfvén waves. *A&A* 394:329–338. <https://doi.org/10.1051/0004-6361:20021135>, [arXiv:astro-ph/0208120](https://arxiv.org/abs/astro-ph/0208120) [astro-ph]
- Varnière P, Tagger M, Rodriguez J (2012) A possible interpretation for the apparent differences in LFQPO types in microquasars. *A&A* 545:A40. <https://doi.org/10.1051/0004-6361/201116698>, [arXiv:1209.3118](https://arxiv.org/abs/1209.3118) [astro-ph.HE]
- Veledina A, Poutanen J (2022) Polarization of comptonized emission in slab geometry. <https://doi.org/10.5281/zenodo.7116125>, URL <https://doi.org/10.5281/zenodo.7116125>
- Veledina A, Muleri F, Dovčiak M, et al (2023) Discovery of X-Ray Polarization from the Black Hole Transient Swift J1727.8-1613. *ApJ* 958(1):L16. <https://doi.org/10.3847/2041-8213/ad0781>, [arXiv:2309.15928](https://arxiv.org/abs/2309.15928) [astro-ph.HE]
- Walton DJ, Reis RC, Cackett EM, et al (2012) The similarity of broad iron lines in X-ray binaries and active galactic nuclei. *MNRAS* 422(3):2510–2531. <https://doi.org/10.1111/j.1365-2966.2012.20809.x>, [arXiv:1202.5193](https://arxiv.org/abs/1202.5193) [astro-ph.HE]

- Walton DJ, Tomsick JA, Madsen KK, et al (2016) The Soft State of Cygnus X-1 Observed with NuSTAR: A Variable Corona and a Stable Inner Disk. *ApJ* 826(1):87. <https://doi.org/10.3847/0004-637X/826/1/87>, [arXiv:1605.03966](https://arxiv.org/abs/1605.03966) [astro-ph.HE]
- Walton DJ, Mooley K, King AL, et al (2017) Living on a Flare: Relativistic Reflection in V404 Cyg Observed by NuSTAR during Its Summer 2015 Outburst. *ApJ* 839(2):110. <https://doi.org/10.3847/1538-4357/aa67e8>, [arXiv:1609.01293](https://arxiv.org/abs/1609.01293) [astro-ph.HE]
- Wang J, Kara E, Steiner JF, et al (2020) Relativistic Reflection and Reverberation in GX 339-4 with NICER and NuSTAR. *ApJ* 899(1):44. <https://doi.org/10.3847/1538-4357/ab9ec3>, [arXiv:1910.01245](https://arxiv.org/abs/1910.01245) [astro-ph.HE]
- Wang J, Mastroserio G, Kara E, et al (2021) Disk, Corona, Jet Connection in the Intermediate State of MAXI J1820+070 Revealed by NICER Spectral-timing Analysis. *ApJ* 910(1):L3. <https://doi.org/10.3847/2041-8213/abec79>, [arXiv:2103.05616](https://arxiv.org/abs/2103.05616) [astro-ph.HE]
- Wang J, Kara E, Lucchini M, et al (2022a) The NICER “Reverberation Machine”: A Systematic Study of Time Lags in Black Hole X-Ray Binaries. *ApJ* 930(1):18. <https://doi.org/10.3847/1538-4357/ac6262>, [arXiv:2205.00928](https://arxiv.org/abs/2205.00928) [astro-ph.HE]
- Wang J, Kara E, García JA, et al (2024) The 2022 Outburst of IGR J17091–3624: Connecting the Exotic GRS 1915+105 to Standard Black Hole X-Ray Binaries. *ApJ* 963(1):14. <https://doi.org/10.3847/1538-4357/ad1595>, [arXiv:2401.10192](https://arxiv.org/abs/2401.10192) [astro-ph.HE]
- Wang PJ, Kong LD, Chen YP, et al (2022b) The 2018 failed outburst of H 1743 - 322: Insight-HXMT, NuSTAR, and NICER views. *MNRAS* 512(3):4541–4555. <https://doi.org/10.1093/mnras/stac773>
- Wang S, Kawai N, Shidatsu M, et al (2018) State transitions of GRS 1739-278 in the 2014 outburst. *PASJ* 70(4):67. <https://doi.org/10.1093/pasj/psy058>, [arXiv:1808.04775](https://arxiv.org/abs/1808.04775) [astro-ph.HE]
- Wang-Ji J, García JA, Steiner JF, et al (2018) The Evolution of GX 339-4 in the Low-hard State as Seen by NuSTAR and Swift. *ApJ* 855(1):61. <https://doi.org/10.3847/1538-4357/aaa974>, [arXiv:1712.02571](https://arxiv.org/abs/1712.02571) [astro-ph.HE]
- Weisskopf MC, Soffitta P, Baldini L, et al (2022) The Imaging X-Ray Polarimetry Explorer (IXPE): Pre-Launch. *Journal of Astronomical Telescopes, Instruments, and Systems* 8(2):026002. <https://doi.org/10.1117/1.JATIS.8.2.026002>, [arXiv:2112.01269](https://arxiv.org/abs/2112.01269) [astro-ph.IM]
- Wijnands R, van der Klis M (2000) The Rapid X-Ray Variability of V4641 Sagittarii (SAX J1819.3-2525 = XTE J1819-254). *ApJ* 528(2):L93–L96. <https://doi.org/10.1086/317110>

1086/312439, [arXiv:astro-ph/9910079](https://arxiv.org/abs/astro-ph/9910079) [astro-ph]

- Wilkins DR, Fabian AC (2011) Determination of the X-ray reflection emissivity profile of 1H 0707-495. *MNRAS* 414(2):1269–1277. <https://doi.org/10.1111/j.1365-2966.2011.18458.x>, [arXiv:1102.0433](https://arxiv.org/abs/1102.0433) [astro-ph.HE]
- Wilkins DR, Fabian AC (2012) Understanding X-ray reflection emissivity profiles in AGN: locating the X-ray source. *MNRAS* 424(2):1284–1296. <https://doi.org/10.1111/j.1365-2966.2012.21308.x>, [arXiv:1205.3179](https://arxiv.org/abs/1205.3179) [astro-ph.HE]
- Xu Y, Harrison FA, García JA, et al (2018) Reflection Spectra of the Black Hole Binary Candidate MAXI J1535-571 in the Hard State Observed by NuSTAR. *ApJ* 852(2):L34. <https://doi.org/10.3847/2041-8213/aaa4b2>, [arXiv:1711.01346](https://arxiv.org/abs/1711.01346) [astro-ph.HE]
- Xu Y, Harrison FA, Tomsick JA, et al (2020a) Evidence for Disk Truncation at Low Accretion States of the Black Hole Binary MAXI J1820+070 Observed by NuSTAR and XMM-Newton. *ApJ* 893(1):42. <https://doi.org/10.3847/1538-4357/ab7cdb>, [arXiv:2003.01778](https://arxiv.org/abs/2003.01778) [astro-ph.HE]
- Xu Y, Harrison FA, Tomsick JA, et al (2020b) Studying the Reflection Spectra of the New Black Hole X-Ray Binary Candidate MAXI J1631-479 Observed by NuSTAR: A Variable Broad Iron Line Profile. *ApJ* 893(1):30. <https://doi.org/10.3847/1538-4357/ab7dc0>, [arXiv:2003.03465](https://arxiv.org/abs/2003.03465) [astro-ph.HE]
- You B, Tuo Y, Li C, et al (2021) Insight-HXMT observations of jet-like corona in a black hole X-ray binary MAXI J1820+070. *Nature Communications* 12:1025. <https://doi.org/10.1038/s41467-021-21169-5>, [arXiv:2102.07602](https://arxiv.org/abs/2102.07602) [astro-ph.HE]
- You B, Cao X, Yan Z, et al (2023) Observations of a black hole x-ray binary indicate formation of a magnetically arrested disk. *Science* 381(6661):961–964. <https://doi.org/10.1126/science.abo4504>, [arXiv:2309.00200](https://arxiv.org/abs/2309.00200) [astro-ph.HE]
- Yuan F, Cui W (2005) Radio-X-Ray Correlation and the “Quiescent State” of Black Hole Sources. *ApJ* 629(1):408–413. <https://doi.org/10.1086/431453>, [arXiv:astro-ph/0411770](https://arxiv.org/abs/astro-ph/0411770) [astro-ph]
- Zdziarski AA, Gierliński M (2004) Radiative Processes, Spectral States and Variability of Black-Hole Binaries. *Progress of Theoretical Physics Supplement* 155:99–119. <https://doi.org/10.1143/PTPS.155.99>, [arXiv:astro-ph/0403683](https://arxiv.org/abs/astro-ph/0403683) [astro-ph]
- Zdziarski AA, Lubiński P, Gilfanov M, et al (2003) Correlations between X-ray and radio spectral properties of accreting black holes. *MNRAS* 342(2):355–372. <https://doi.org/10.1046/j.1365-8711.2003.06556.x>, [arXiv:astro-ph/0209363](https://arxiv.org/abs/astro-ph/0209363) [astro-ph]
- Zdziarski AA, Ziolkowski J, Mikołajewska J (2019) The X-ray binary GX 339-4/V821 Ara: the distance, inclination, evolutionary status, and mass

- transfer. MNRAS 488(1):1026–1034. <https://doi.org/10.1093/mnras/stz1787>, [arXiv:1904.07803](https://arxiv.org/abs/1904.07803) [astro-ph.SR]
- Zdziarski AA, Jourdain E, Lubiński P, et al (2021) Hybrid Comptonization and Electron-Positron Pair Production in the Black-hole X-Ray Binary MAXI J1820+070. ApJ 914(1):L5. <https://doi.org/10.3847/2041-8213/ac0147>, [arXiv:2104.04316](https://arxiv.org/abs/2104.04316) [astro-ph.HE]
- Zdziarski AA, Chand S, Banerjee S, et al (2024) What Is the Black Hole Spin in Cyg X-1? ApJ 967(1):L9. <https://doi.org/10.3847/2041-8213/ad43ed>, [arXiv:2402.12325](https://arxiv.org/abs/2402.12325) [astro-ph.HE]
- Zdziarski AA, Banerjee S, Szanecki M, et al (2025) Is the Spin of the Black Hole in GX 339–4 Negative? ApJ 981(1):L15. <https://doi.org/10.3847/2041-8213/adb62e>, [arXiv:2412.15705](https://arxiv.org/abs/2412.15705) [astro-ph.HE]
- Zhan Y, You B, Ingram A, et al (2025) Modeling fast X-ray variability around an accreting black hole. arXiv e-prints arXiv:2502.03995. <https://doi.org/10.48550/arXiv.2502.03995>, [arXiv:2502.03995](https://arxiv.org/abs/2502.03995) [astro-ph.HE]
- Zhang SN, Cui W, Chen W (1997) Black Hole Spin in X-Ray Binaries: Observational Consequences. ApJ 482(2):L155–L158. <https://doi.org/10.1086/310705>, [arXiv:astro-ph/9704072](https://arxiv.org/abs/astro-ph/9704072) [astro-ph]
- Zhang SN, Feroci M, Santangelo A, et al (2016) eXTP: Enhanced X-ray Timing and Polarization mission. p 99051Q, <https://doi.org/10.1117/12.2232034>, [arXiv:1607.08823](https://arxiv.org/abs/1607.08823)
- Zhang SN, Santangelo A, Xu Y, et al (2025) The enhanced X-ray Timing and Polarimetry mission—eXTP for launch in 2030. Science China Physics, Mechanics, and Astronomy 68(11):119502. <https://doi.org/10.1007/s11433-025-2786-6>, [arXiv:2506.08101](https://arxiv.org/abs/2506.08101) [astro-ph.HE]
- Zhang W, Dovčiak M, Bursa M (2019) Constraining the Size of the Corona with Fully Relativistic Calculations of Spectra of Extended Coronae. I. The Monte Carlo Radiative Transfer Code. ApJ 875(2):148. <https://doi.org/10.3847/1538-4357/ab1261>, [arXiv:1903.09241](https://arxiv.org/abs/1903.09241) [astro-ph.HE]
- Zhang Y, Méndez M, García F, et al (2022) The evolution of the corona in MAXI J1535-571 through type-C quasi-periodic oscillations with Insight-HXMT. MNRAS 512(2):2686–2696. <https://doi.org/10.1093/mnras/stac690>, [arXiv:2203.05308](https://arxiv.org/abs/2203.05308) [astro-ph.HE]
- Zhang Y, Méndez M, García F, et al (2023) A NICER look at the jet-like corona of MAXI J1535-571 through type-B quasi-periodic oscillations. MNRAS 520(4):5144–5156. <https://doi.org/10.1093/mnras/stad460>, [arXiv:2302.04007](https://arxiv.org/abs/2302.04007) [astro-ph.HE]

- Zhang Z, Thomsen LL, Dai L, et al (2024) Modeling Multiple X-Ray Reflection in Super-Eddington Winds. *ApJ* 977(2):157. <https://doi.org/10.3847/1538-4357/ad86c0>, [arXiv:2407.08596](https://arxiv.org/abs/2407.08596) [astro-ph.HE]
- Zhao QC, Dovčiak M, Li H, et al (2026) The First X-Ray Polarimetry of GRS 1739–278 Reveals Its Rapidly Spinning Black Hole. *ApJ* 997(1):L12. <https://doi.org/10.3847/2041-8213/ae3182>, [arXiv:2512.21899](https://arxiv.org/abs/2512.21899) [astro-ph.HE]
- Zhao X, Gou L, Dong Y, et al (2021) Re-estimating the Spin Parameter of the Black Hole in Cygnus X-1. *ApJ* 908(2):117. <https://doi.org/10.3847/1538-4357/abbc66>, [arXiv:2102.09093](https://arxiv.org/abs/2102.09093) [astro-ph.HE]
- Zhou M, Abdikamalov AB, Ayzenberg D, et al (2019) XSPEC model for testing the Kerr black hole hypothesis using the continuum-fitting method. *Phys. Rev. D* 99(10):104031. <https://doi.org/10.1103/PhysRevD.99.104031>, [arXiv:1903.09782](https://arxiv.org/abs/1903.09782) [gr-qc]
- Zhu Y, Davis SW, Narayan R, et al (2012) The eye of the storm: light from the inner plunging region of black hole accretion discs. *MNRAS* 424(4):2504–2521. <https://doi.org/10.1111/j.1365-2966.2012.21181.x>, [arXiv:1202.1530](https://arxiv.org/abs/1202.1530) [astro-ph.HE]
- Zoghbi A, Fabian AC, Reynolds CS, et al (2012) Relativistic iron K X-ray reverberation in NGC 4151. *MNRAS* 422(1):129–134. <https://doi.org/10.1111/j.1365-2966.2012.20587.x>, [arXiv:1112.1717](https://arxiv.org/abs/1112.1717) [astro-ph.HE]
- Zoghbi A, Cackett EM, Reynolds C, et al (2014) Observations of MCG-5-23-16 with Suzaku, XMM-Newton and NuSTAR: Disk Tomography and Compton Hump Reverberation. *ApJ* 789(1):56. <https://doi.org/10.1088/0004-637X/789/1/56>, [arXiv:1405.3674](https://arxiv.org/abs/1405.3674) [astro-ph.HE]